NAVAL POSTGRADUATE SCHOOL

MONTEREY, CALIFORNIA

THESIS

MODELING AND INVESTIGATION OF HEAVY OXIDE AND ALKALI-HALIDE SCINTILLATORS FOR POTENTIAL USE IN NEUTRON AND GAMMA DETECTION SYSTEMS

by

Jeremy S. Cadiente

June 2015

Thesis Advisor: Craig F. Smith
Second Reader: Tim Goorley

Approved for public release; distribution is unlimited

THIS PAGE INTENTIONALLY LEFT BLANK

Public reporting burden for this collection of information is estimated to average 1 hour per response, including the time for reviewing instruction, searching existing data sources, gathering and maintaining the data needed, and completing and reviewing the collection of information. Send comments regarding this burden estimate or any other aspect of this collection of information, including suggestions for reducing this burden, to Washington headquarters Services, Directorate for Information Operations and Reports, 1215 Jefferson Davis Highway, Suite 1204, Arlington, VA 22202–4302, and to the Office of Management and Budget, Paperwork Reduction Project (0704–0188) Washington DC 20503.

1. AGENCY USE ONLY *(Leave blank)*	2. REPORT DATE June 2015	3. REPORT TYPE AND DATES COVERED Master's Thesis

4. TITLE AND SUBTITLE MODELING AND INVESTIGATION OF HEAVY OXIDE AND ALKALI-HALIDE SCINTILLATORS FOR POTENTIAL USE IN NEUTRON AND GAMMA DETECTION SYSTEMS	5. FUNDING NUMBERS
6. AUTHOR(S) Jeremy S. Cadiente	

7. PERFORMING ORGANIZATION NAME(S) AND ADDRESS(ES) Naval Postgraduate School Monterey, CA 93943–5000	8. PERFORMING ORGANIZATION REPORT NUMBER

9. SPONSORING /MONITORING AGENCY NAME(S) AND ADDRESS(ES) N/A	10. SPONSORING/MONITORING AGENCY REPORT NUMBER

11. SUPPLEMENTARY NOTES The views expressed in this thesis are those of the author and do not reflect the official policy or position of the Department of Defense or the U.S. Government. IRB Protocol number ____N/A____.

12a. DISTRIBUTION / AVAILABILITY STATEMENT Approved for public release; distribution is unlimited	12b. DISTRIBUTION CODE

13. ABSTRACT (maximum 200 words)

Heavy inorganic oxide and alkali-halide crystals, which previous experimental research has indicated to have fast neutron detection efficiencies well over 40%, were investigated for potential use as highly efficient gamma-neutron radiation detectors. The Monte Carlo N-Particle radiation transport code (MCNP) was used to characterize the radiation interactions in a candidate set of crystals, including Bismuth Germanate (BGO), Lead Tungstate (PWO), Cadmium Tungstate (CWO), Zinc Tungstate (ZWO), Cerium-doped Lutetium-Gadolinium Orthosilicate (LGSO:Ce), and Cerium doped Lutetium-Aluminum Garnet (LuAG:Ce). Specific detection systems proposed and studied in the laboratory were also modeled and assessed.

The candidate crystal set proved to be most susceptible to energy deposition from incident gamma quanta below 0.7 MeV and above 4 MeV, most likely due to photoelectric absorption and pair production, respectively. Inelastic and elastic scattering proved to be about 98% of the total neutron interactions from a Plutonium Beryllium (PuBe) neutron source, about a fourth of which were inelastic scattering. Various components of the detector configuration were evaluated in detail. The crystal dimensions and moderation especially affected detector efficiency, which showed potential for detection efficiencies comparable to experimental data.

14. SUBJECT TERMS Inelastic scattering, neutron radiation, gamma radiation, inorganic scintillators, MCNP, detection efficiency, neutron detection	15. NUMBER OF PAGES 71
	16. PRICE CODE

17. SECURITY CLASSIFICATION OF REPORT Unclassified	18. SECURITY CLASSIFICATION OF THIS PAGE Unclassified	19. SECURITY CLASSIFICATION OF ABSTRACT Unclassified	20. LIMITATION OF ABSTRACT UU

i

THIS PAGE INTENTIONALLY LEFT BLANK

MODELING AND INVESTIGATION OF HEAVY OXIDE AND ALKALI-HALIDE SCINTILLATORS FOR POTENTIAL USE IN NEUTRON AND GAMMA DETECTION SYSTEMS

Jeremy S. Cadiente
Ensign, United States Navy
B.S., United States Naval Academy, 2014

Submitted in partial fulfillment of the
requirements for the degree of

MASTER OF SCIENCE IN APPLIED PHYSICS

from the

**NAVAL POSTGRADUATE SCHOOL
June 2015**

Author: Jeremy S. Cadiente

Approved by: Craig F. Smith
                Thesis Advisor

                Tim Goorley
                Second Reader

                Andres Larraza
                Chair, Department of Physics

THIS PAGE INTENTIONALLY LEFT BLANK

ABSTRACT

Heavy inorganic oxide and alkali-halide crystals, which previous experimental research has indicated to have fast neutron detection efficiencies well over 40%, were investigated for potential use as highly efficient gamma-neutron radiation detectors. The Monte Carlo N-Particle radiation transport code (MCNP) was used to characterize the radiation interactions in a candidate set of crystals, including Bismuth Germanate (BGO), Lead Tungstate (PWO), Cadmium Tungstate (CWO), Zinc Tungstate (ZWO), Cerium-doped Lutetium-Gadolinium Orthosilicate (LGSO:Ce), and Cerium doped Lutetium-Aluminum Garnet (LuAG:Ce). Specific detection systems proposed and studied in the laboratory were also modeled and assessed.

The candidate crystal set proved to be most susceptible to energy deposition from incident gamma quanta below 0.7 MeV and above 4 MeV, most likely due to photoelectric absorption and pair production, respectively. Inelastic and elastic scattering proved to be about 98% of the total neutron interactions from a Plutonium Beryllium (PuBe) neutron source, about a fourth of which were inelastic scattering. Various components of the detector configuration were evaluated in detail. The crystal dimensions and moderation especially affected detector efficiency, which showed potential for detection efficiencies comparable to experimental data.

THIS PAGE INTENTIONALLY LEFT BLANK

TABLE OF CONTENTS

THIS PAGE INTENTIONALLY LEFT BLANK

LIST OF FIGURES

LIST OF TABLES

THIS PAGE INTENTIONALLY LEFT BLANK

LIST OF ACRONYMS AND ABBREVIATIONS

A	atomic mass number
BGO	bismuth Germinate ($Bi_4Ge_3O_{12}$)
Ce	cerium
CWO	cadmium tungstate ($CdWO_4$)
DTRA	Defense Threat Reduction Agency
ISM	Institute of Scintillation Materials
LET	linear energy transfer
LGSO	lutetium gadolinium orthosilicate ($Lu_2Gd_2SiO_5$)
LuAG	lutetium aluminum garnet ($Lu_3Al_5O_{12}$)
MCNP	Monte Carlo N-Particle
NASU	National Academy of Sciences of Ukraine
Pb	lead
PMT	photomultiplier tube
PuBe	Plutonium beryllium
PWO	lead tungstate ($PbWO_4$)
RM	Radioactive Material
YSO	Yttrium orthosilicate (Y_2SiO_5)
Z	atomic number
Zeff	effective atomic number
ZWO	zinc tungstate ($ZnWO_4$)

THIS PAGE INTENTIONALLY LEFT BLANK

ACKNOWLEDGMENTS

I would, first and foremost, like to thank my friends and family for their continued support and encouragement in this endeavor as much as in all the rest. I would especially like to thank my mother, Mary; Darryl and Bette Christian; Mike Buck; Patrick O'Boyle; and my wife, Lisa, for their undeserved belief in me.

I extend a sincere thank you to my NPS research advisor, Professor Craig Smith, for the opportunity to work with him, as well as his constant teaching and guidance along the way. You have made this experience a positive and eye-opening one. I would like to express my sincere gratitude to Dr. Tim Goorley and the XCP Division of Los Alamos National Lab for their eagerness to share their technical expertise and insights throughout this entire endeavor. It has truly been a pleasure working with you again. I would also like to acknowledge support from the Nuclear Science and Engineering Research Center (NSERC) and the Defense Threat Reduction Agency (DTRA).

Thank you to the United States Naval Academy Admiral Frank Bowman Scholarship program for this opportunity to come to the Naval Postgraduate School. This has been a rewarding experience that I am sure will enable me to serve the Fleet in a greater capacity.

Finally, thank you to the One who makes all things possible.

THIS PAGE INTENTIONALLY LEFT BLANK

I. INTRODUCTION

A. MOTIVATION

Since 2002, the National Security Strategy of the United States of America has called for "proactive counterproliferation efforts" and "strengthened nonproliferation efforts to prevent rogue states and terrorists from acquiring materials, technologies, and expertise necessary for weapons of mass destruction (WMD)" [1]. While the nuclear threat from major world powers has decreased significantly since the Cold War Era, the threat from rogue states and terrorists has come increasingly into focus in the past decade [2]. Part of that effort is the creation of the Defense Threat Reduction Agency (DTRA), a combat support agency responsible to the Assistant to the Secretary of Defense for countering nuclear, chemical, biological, and high explosive WMD [3]. In this research, the Naval Postgraduate School (NPS) is coming alongside DTRA in its efforts to develop novel methods and applications for detection of nuclear weapons and materials. This thesis will address a specific application for fast neutron detection.

The research focus is the use of heavy, inorganic oxide solid-state scintillation detectors for the detection of a mixed radiation source of fast neutrons and gamma rays. Experiments with inorganic crystals with high-atomic number constituents have unusually high detection efficiency of fast neutrons as a result of inelastic scattering [4]. Much work has been done both at NPS and the Institute of Scintillation Materials (ISM) of the National Academy of Sciences of Ukraine (NASU) to demonstrate gamma detection efficiency up to 80% and fast neutron detection efficiency well above 40% for heavy oxide inorganic crystals, while organic and liquid-based scintillators typically have fast neutron detection efficiencies below 10% [5]. This significant increase in detection efficiency of both high energy gamma quanta and fast neutrons by the same detector would greatly increase the detector sensitivity and significantly lower its size and cost [4]. The particular crystals in this study are Bismuth Germanate (BGO), Lead Tungstate (PWO), Cadmium Tungstate (CWO), Zinc Tungstate (ZWO), Cerium-doped Lutetium-Gadolinium Orthosilicate (LGSO:Ce), and Cerium doped Lutetium-Aluminum Garnet (LuAG:Ce), as summarized in Table 1. The applications for detectors based on such

scintillator crystals are broad, including radioactive material detection at international border checkpoints, shipping ports, and major, high-occupancy events. Detection systems currently being used to detect radioactive material (RM) rely on bulky assemblies consisting of components such as organic scintillator detectors for gamma detection and ^{3}He detectors inside polyethylene moderators for neutron thermalization and detection [4]. These systems have several disadvantages. ^{3}He-based detectors have very low detection efficiency (around 0.8%) for fast neutrons without moderators, around 10% detection efficiency with moderation, and require detector panels that are large in volume and mass for registration of weak neutron fluxes [4]. The use of heavy, inorganic scintillator crystals for direct detection of fast neutrons, however, shows potential for more efficient, less expensive, and more portable RM detection systems.

Table 1.   Candidate set of scintillator crystals obtained from the Institute for Scintillation Materials, Ukraine

Scintillator material	Chemical Formula	Abbreviation	Dimensions (mm)	Activated	Density (g/cc)
Bismuth Germanate	$Bi_4Ge_3O_{12}$	BGO	20x30x11	No	7.13
Lead Tungstate	$PbWO_4$	PWO	22x22x10	No	8.28
Cadmium Tungstate	$CdWO_4$	CWO	20x20x20	No	7.9
Zinc Tungstate	$ZnWO_4$	ZWO	20x20x20	No	7.87
Lutetium-Gadolinium Orthosilicate	$Lu_2Gd_2SiO_5(Ce)$	LGSO:Ce	20(dia) x 10	Yes, 0.3% Cerium	7.0
Lutetium-Aluminum Garnet	$Lu_3Al_5O_{12}(Ce)$	LuAG:Ce	20(dia) x 10	Yes, 0.001% Cerium	6.73

Although significant empirical data for the response of such crystals has been accumulated in the laboratory, there has been less effort to understand the radiation-scintillator interaction processes for this novel approach to fast neutron detection through state-of-the-art Monte Carlo simulation and modeling methods.

B.   APPROACH

While previous work in this effort, by both ISM-NASU and NPS, has been predominantly experimental, this thesis is an investigation of the candidate set of crystals from a computational approach. The designated tool is the Monte Carlo N-Particle (MCNP) radiation transport code [6], which uses statistical characterization of radiation transport processes combined with libraries of atomic and nuclear data to simulate physical phenomena, including the relevant radiation-matter interactions. All computational work is done with MCNP6, Version 1.0. MCNP is widely considered the international "gold standard" for particle radiation transport codes in diverse areas, including nuclear physics, commercial industries, and medical science.

The approach taken is to model specific lab set ups and experiments done both at NPS and in Ukraine to verify and develop crystal-specific data and gain a more robust understanding of the physical processes taking place in the crystals. This includes the creation of specific experimental set ups, including geometrical dimensions, source specifications, and material description. Once the radiation transport simulation has run, certain calculations require post-processing of the output file to extract desired data.

C.   RESEARCH OBJECTIVES AND GOALS

The over-arching objective of this research effort is to understand how these heavy oxide and alkali-halide crystals react to a mixed radiation source of neutrons (fast and thermal) and gammas. In an attempt to develop this understanding, this thesis will address the following.

1.   What radiation-matter interactions occur inside the crystals?

Previous experiments on these crystals have produced data that indicate high detection efficiencies, but the physical mechanisms by which the radiation is detected have only been inferred from theory. In a computational model, what interactions occur between fast neutrons and the crystals? What interactions occur been thermal neutrons and the crystals? What interactions occur between gamma rays and the crystals? How many collisions are there? How do these interactions depend on the energy of the incident radiation? Of these interactions, which deposit the most energy?

2.   Calculate energy deposition.

How much energy was deposited in previous experiments at NPS? How does the energy deposition from each radiation source depend on energy of incident radiation?

3.   What components of the proposed detection system optimize detection efficiency of a mixed gamma-neutron radiation source?

What role does shielding play in neutron detection? What role does neutron moderation play? How do the scintillator crystal dimensions affect their overall effectiveness as neutron detectors?

4.   What detection efficiency is possible for each of these crystals?

For each configuration, the ratio of particles that interact with the scintillator material to the total number of particles entering the crystal material gives an estimate of the potential intrinsic efficiency for each crystal. This estimation makes a critical assumption that every incident particle that has an interaction produces a detectable signal. Because this is not always the case, this estimate serves as an upper limit to the achievable intrinsic counting efficiency.

II.   BACKGROUND PHYSICS

When radiation interacts with the material inside a scintillation detector, energy is transferred to the material through various interaction mechanisms. The energy deposited into the scintillating material in these processes produces a signal at the detector output. Radiation exists in many forms, each with its own set of interaction mechanisms. The main forms of radiation emitted from typical fissile nuclear materials are gamma quanta and neutrons, both of which, experimental analysis indicate, can be detected within the same heavy-oxide detector [4]. This chapter will discuss relevant interaction mechanisms associated with gamma and neutron radiation and the process by which those interactions are detected in a scintillator.

A.   GAMMA RADIATION

Gamma rays are a form of high energy electromagnetic radiation created in a nuclear process or transition. Gamma radiation from the decay of radioactive materials typically ranges up to a few MeV in energy, with no theoretical upper limit. Unlike charged particles, gamma radiation does not transfer energy continuously, but rather scatters off or becomes absorbed through individual ionization and excitation events as it travels through a material [9]. As the gamma rays enter a scintillator medium, the fraction that are absorbed by one of these events is defined by

$$f = 1 - e^{(-\mu d)} \tag{1}$$

where μ is the summation of linear attenuation coefficients (τ, σ, κ) in, $cm^{(-1)}$, from three major interactions as the rays travel a distance d into the scintillator [9]. The three interactions for those coefficients are photoelectric absorption, Compton scattering, and pair production, respectively, each of which is discussed shortly. The values of these coefficients are dependent on not only the energy of the incident gamma photon, but also the physical properties of the scintillator material.

1. Photoelectric Absorption

The photoelectric effect is a process by which a gamma ray becomes absorbed by a bound electron. In this process, all of the gamma energy is transferred into overcoming the bound state of the electron and additional incident gamma energy converts to the kinetic energy of the freed electron, shown as

$$E_{e^-} = h v - E_b \tag{2}$$

where v is the frequency of the incoming gamma and E_b is the energy of the bound state of the electron. Furthermore, the vacancy left by the freed electron is quickly filled by surrounding free-electrons and/or by the reshuffling of electrons in other shells of the atom, often generating characteristic X-ray photons in the process [9]. Photoelectric absorption is the dominant gamma-matter interaction at low photon energies, which will be below roughly 0.75 MeV for the heavy oxide crystals under investigation. The probability of this interaction also has a strong dependence on atomic number, so this mechanism is expected to be a dominant event in this candidate set of high-Z crystals at energies below 2 MeV [10].

2. Compton Scattering

When a gamma ray photon elastically collides with a bound electron whose energy is extremely low compared to that of the gamma, the Compton effect takes place [9]. Unlike photoelectric absorption, not all of the photon energy is used up; rather a portion of it accelerates the electron as the gamma ray scatters off with a reduced energy

$$E' = \frac{E}{1 + \alpha (1 - cos\theta)} \tag{3}$$

where α is a ratio of the initial photon energy to the electron rest-mass energy and θ is the angle the photon scatters measured from its original direction [9].

The cross section for Compton scattering by electrons in scintillator atoms depends on the number of available electrons in the medium and, therefore, increases linearly with Z [10]. While the probability of Compton scattering increases with

decreasing gamma energy, this trend is much stronger with photoelectric absorption at lower energies and so the latter is expected to dominate in this part of the energy spectrum (see Figure 1).
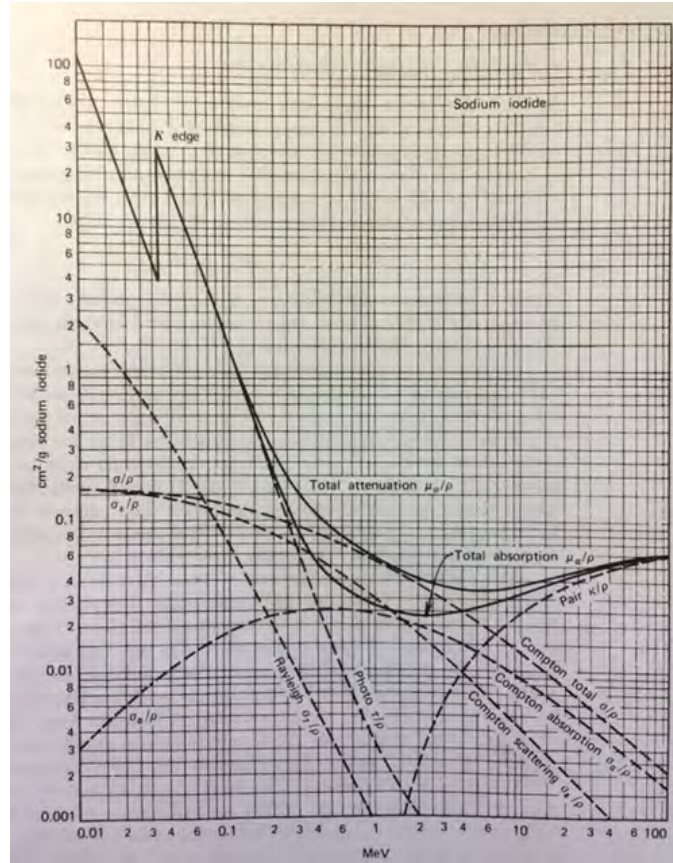
Figure 1.   Cross sections for gamma interactions with sodium iodide vs. incident gamma energy, from [9].

3.   Pair Production (high E, >1 MeV)

When the incident energy of the gamma-ray photon exceeds twice the rest-mass energy of an electron (1.02 MeV), there is a possibility that the gamma is completely absorbed in the creation of an electron and a positron through the phenomenon of pair production (i.e., the creation of an electro-positron pair). In this event, which is almost always confined to the coulomb field of a nucleus, excess energy from the incident gamma is converted into the kinetic energy shared by the pair according to

$$T_{pp} = E - 2E_e \tag{4}$$

where T_{pp} is the kinetic energy of the pair and E_e is rest-mass energy of an electron [8]. As the resultant positron loses energy in the medium it will eventually annihilate with another electron and produce two secondary annihilation photons, which can affect the response of the detector [10].

While there is no simple equation for the probability of pair production, there are certain trends as depicted in Figure 1. Most notable is that, though pair production becomes possible at incident energies greater than 1.02 MeV, its cross section rises quickly with increasing energy and only becomes significant at several MeV. As seen in Figure 2, the energy dependence itself is heavily affected by the atomic number of the scintillator crystal.
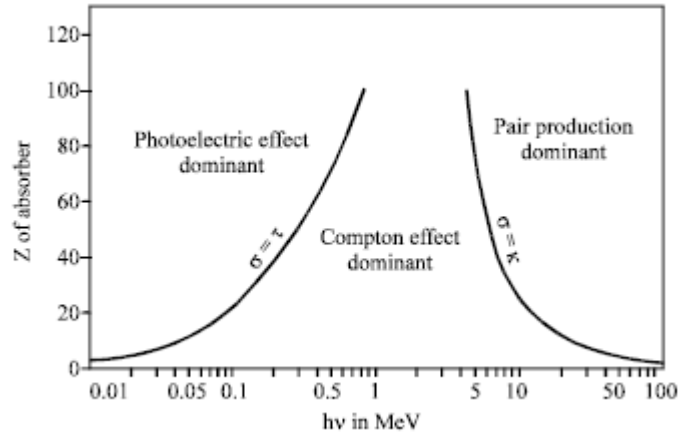
Figure 2.   Behavior of gamma interaction with matter with respect to Z number and incident gamma energy. Solid lines mark equal probability of processes, from [10].

The attenuation coefficients for each of these gamma-matter interactions vary based on the physical properties of the scintillation crystals and the energy of the incident radiation. Each interaction yields secondary electrons and residual photons that are related to the incident energy E in different ways, resulting in multiple absorption interactions [9]. In general, the approach to obtain increased detection in a scintillation

8

counter is to increase the dimensions of the absorbing crystal in order to obtain optimal absorption efficiency.

B.   NEUTRON RADIATION

Neutron radiation is sectioned into four main categories based on energy, as shown in Table 2. Neutrons do not carry charge and, therefore, do not interact with the electron clouds of the atoms of the absorbing material in contrast with some other types of radiation, but rather pass through to interact with the atomic nuclei [9]. There are two primary possibilities for this interaction: absorption and scattering.

Table 2.   Categories of neutron radiation by energy, from [11].

Nomenclature	Energy
Thermal	≈ 0.025 eV
Epithermal	~ 1 eV
Slow	~ 1 keV
Fast	= 100 keV–10 MeV

1.   Neutron Absorption

The detection of slow or thermal neutrons is chiefly done through the process of neutron absorption. At sufficiently low neutron energies (typically in the slow neutron region or below), there is a significant probability that the nuclei absorbsthe neutron. The result is a new excited recoil nucleus and a series of processes that are fundamental to the detection of the original incident neutron. The most probable neutron-induced reaction for most materials, especially those heavy nuclei constituents, is radiative capture reaction (n, γ). This reaction typically produces gamma radiation that can be detected directly. The decay of the resulting excited nucleus emits several particles, including

gamma-quanta, beta particles, alpha partcles, and protons. These emissions can also provide for indirect detection of neutrons [10].

Additionally, detection of slow neutrons can also be done through neutron-induced reactions that emit heavier, charged particles such as alpha particles. With very heavy nuclei (Z > 90), neutron capture can erupt in nuclear fission and the highly kinetic fissile fragments are detected. When slightly lighter nuclei, such as those that comprise the crystal set under investigation, absorb a neutron they can undergo nuclear reactions that emit charged particles, typically alpha particles [9]. Two well-known reactions of this sort that are often used in scintillation detection of slow neutrons are

$$B^{10}(n,\alpha)Li^7 \tag{5}$$

and

$$Li^6(n,\alpha)H^3, \tag{6}$$

the cross sections of which are plotted as a function of neutron energy in Figure 3 [9, pp. 36–38]. As seen in Figure 3, the cross sections of both reactions display strong energy dependence as they decrease roughly as 1/v, where v is the neutron velocity.
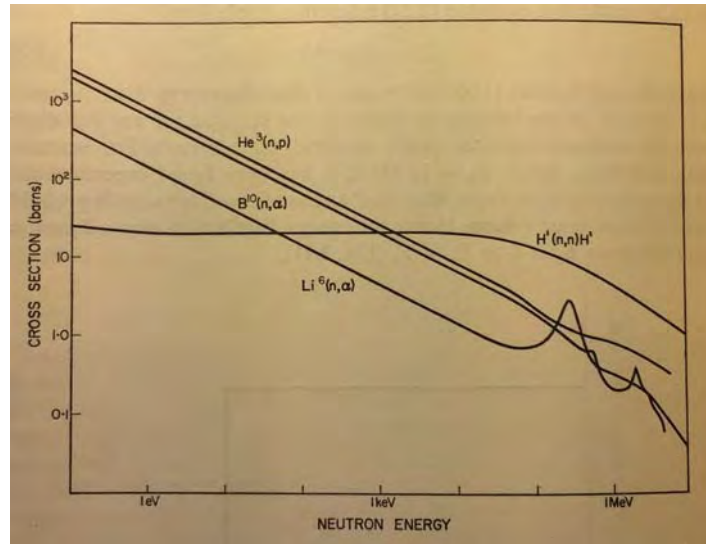
Figure 3.   Log-log plot of neutron absorption or scattering cross sections for four neutron detection process vs. neutron energy, from [9].

10

Because charged particles, such as alphas, interact with the Coulomb fields of the crystal atoms, they have a much larger linear energy transfer (LET), making direct detection much easier than that of gamma emissions. However, the probability of any neutron-induced reaction falls off quickly with increasing neutron energy (as shown in the right hand side of the figure above) limiting neutron detection via absorption at the keV energy level.

2. Neutron Scattering

Neutron scattering, unlike absorption, changes the energy and direction of the neutron without altering the proton and neutron number of the nucleus. This type of interaction is further divided into elastic and inelastic scattering. Elastic scattering is a collision in which the incoming neutron transfers a fraction of its kinetic energy to the target nuclei, yet there is a conservation of kinetic energy within the two-particle system. The average energy loss by the neutron during this collision is given by

$$E'_{avg} = \frac{2EA}{(A+1)^2} \tag{7}$$

where E is the incident kinetic energy of the neutron and A is the atomic mass of the nuclei [8]. This relation reveals that less massive (lighter) nuclei are considerably more effective at moderating, or slowing down, neutrons. This elastic process results in the previously at rest nucleus now traveling through the surrounding matter as a heavy charged particle with high LET, which can be detected.

At sufficiently high neutron energies, inelastic scattering can take place. In this case, the kinetic energy of the neutron and nucleus is not conserved, but rather some of the neutron energy is expended in exciting the nucleus. Almost immediately, the recoil nucleus de-excites back down the ground state and that energy is converted into gamma radiation. For inelastic scattering to be possible, the kinetic energy of the incoming neutron must be large enough to bring the nucleus to an excited state. This so called threshold energy, E_{th}, depends on several factors, including the atomic number Z and density of possible excitation levels of the target nuclei, but is typically above 1 MeV.

11

Figure 4 displays the Z dependence of inelastic scattering cross sections, along with that of the total scattering cross section. At 4–7 MeV, inelastic scattering is roughly 35%–45% of the all interactions, depending on the atomic number of target nuclei. Figure 4 is simplified in the sense that each individual isotope actually has 10s of possible inelastic reactions, each with a different neutron threshold and different gamma emissions that correspond to distinct excited nuclear states. Due to the complexity related to the energy levels of the nucleus, there is no simple expression for average energy loss as was shown with elastic scattering, but the general effect is higher energy loss by the neutron [8].
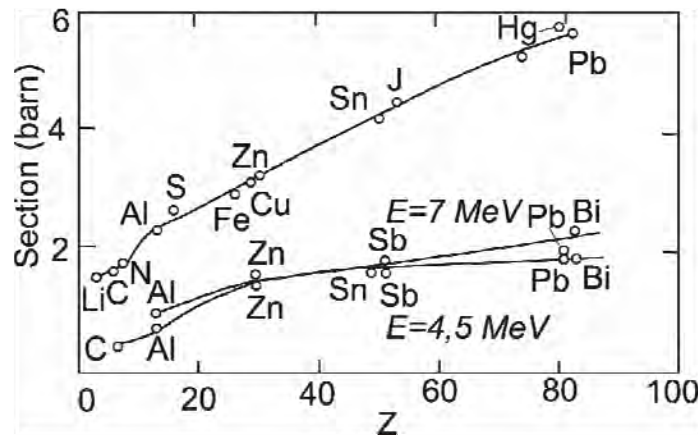
Figure 4.   Cross section of total interactions (top line) and inelastic scattering (bottom 2 lines) of various elements vs. atomic number, at neutron energy of 7, 5, and 4 MeV, from [6].

A typical method of fast neutron detection is based on elastic scattering, called proton recoil detectors. In these detectors, inelastic scattering serves the role of moderating high energy neutron to such an energy at which detection via elastic scattering can take place, but the accompanying secondary radiation from inelastic scattering is seen as unwanted complication in the detector response [10, pp. 56, 553]. The proposed method of employing heavy inorganic scintillators, however, utilizes inelastic scattering within the crystals to more directly detect fast neutrons, removing the requirement for moderation. The advantages are an immediate response and increased efficiency with high-Zeff crystals.

C.   SCINTILLATION THEORY

Scintillation is the process in which a scintillator material stimulated by ionizing radiation gives off energy in the form of light emission. This process in inorganic crystals, known as luminescence, is based on the energy states of the crystalline structure of the material. Each atom or molecule in an inorganic crystal lattice has an electronic system of discrete energy levels governed by Schrödinger's equation resulting in a series of energy bands for the bulk material, as shown in Figure 5 [9, pp.68–70]. Because of the quantum mechanical nature of these electrons, groups of energy states, or bands, are "forbidden" in the sense that they cannot be occupied by a charge carrier. Conversely, electrons within an allowed energy state moves freely within that state.
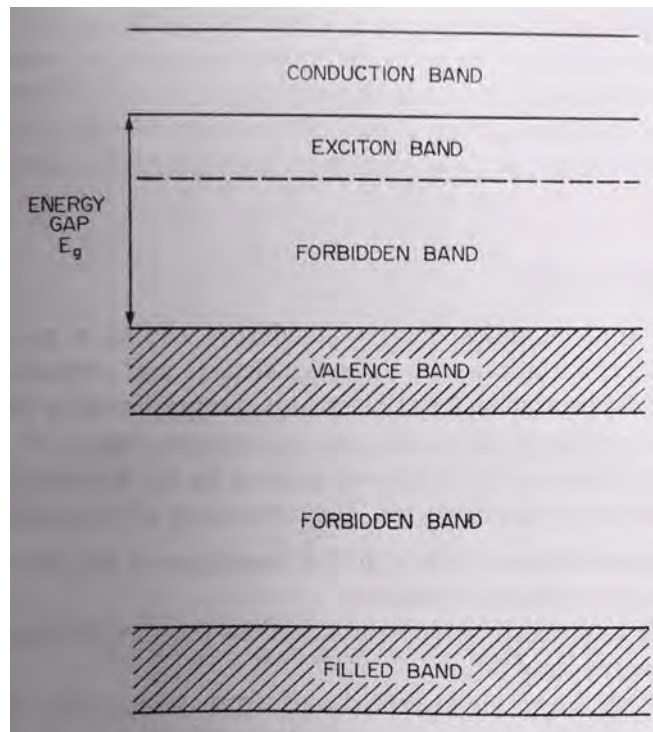
Figure 5.   Energy band structure of ideal insulating crystal, from [9].

The highest band of completely filled states is referred to as the "valence band." Upon perturbation of this valence band, electrons can become excited into the "conduction band," but must overcome the energy band gap E_g of the system to do so.

13

Since a positively charged "hole" is left in the valence band, this process creates an electron-hole pair. Sometimes, the electron-hole pair remains bound, creating what is known as an exciton. Electrons promoted to the exciton band are free to move in the lattice crystal, but full ionization has not occurred and therefore they carry no net charge [9]. When electrons or excitons drop from their excited bands back to the valence band and energy in the form of a photon is emitted, scintillation has occurred (Figure 6).
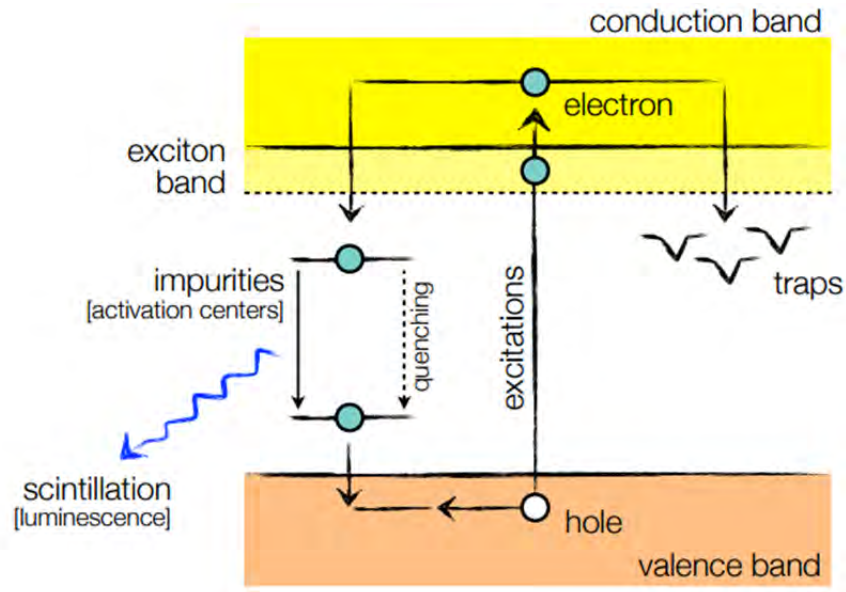
Figure 6.   Scintillation, quenching, and trapping processes in an inorganic crystal structure. from [12].

1.   Activators and Fast Component

Electrons (or excitons) in the conduction (or exciton) band typically undergo one or more of three main processes: luminescence, quenching, or trapping. While luminescence, or scintillation, is the desired response of the material, it is a highly inefficient process in most pure crystals. Additionally, it is common for energy bandgaps to be so large that the emitted photon is outside of the visible range [10, p. 232]. To overcome this and increase luminescence probability, small concentrations of impurities, called activators, are added to the crystals, as in the case of the LGSO:Ce and LUAG:Ce crystals in this study. Activators create intermediate discrete energy levels within the

14

forbidden band from which the electrons/excitons can de-excite to the valence band. Two things are required for these intermediate excitation states, known as "activation centers (shown in Figure 6): the capture of an electron from the conduction band and the capture of hole from the valence band [12]. This can happen by the recombination of an electron and a hole or the simultaneous capture of an exciton from the exciton band [9, p. 71]. These excited states have half-lives typically on the order of 50–500 ns, resulting in the fast component of response of inorganic scintillators [10]. Furthermore, the energy band gap from activation centers is smaller than that of the forbidden gap, and thus the photon emitted during relaxation is more likely to be in the visible range.

2.   Trapping, Slow Component, and Quenching

Trapping occurs as a result of intermediate metastable levels below the conduction band due to defects and disturbances in the crystal lattice [9, pp. 72–73]. These traps can capture electrons from the conduction band, preventing them from dropping back to the valence band through scintillation. Instead, electrons/excitons in traps can receive additional excitation energy and move up to the conduction band again. This is often done via thermal excitation. By moving back into the conduction band, the electron regains the opportunity to de-excite to the ground state. This trapping process can create a significant delay in the scintillation of the material, resulting in a slow component of light, called phosphorescence, depicted in Figure 7 [10, pp. 231–233], [12].
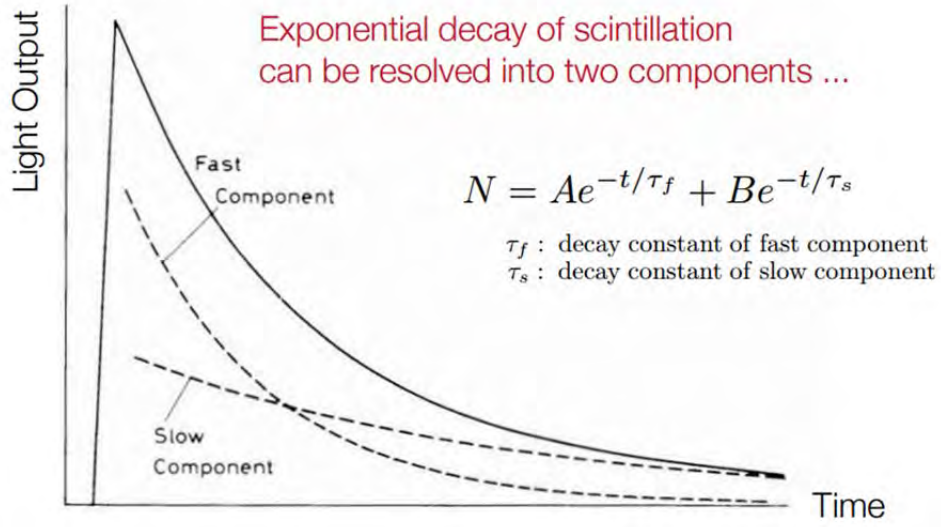
Figure 7.   The total relaxation of luminescent crystal shown as sum of slow
and fast exponential decay, from [11].

Quenching is the third process undergone by electrons in the conduction band. Not all electrons in traps are re-excited to the conduction band and not all electrons in activation centers result in scintillation. Some excitation states within the forbidden band have a sufficiently small energy bandgap to the ground state that the electron may de-excite in radiationless transitions, called quenching [10]. Quenching dissipates the excess energy thermally, competing with luminescent transitions that are useful in detection. Luminescence quantum efficiency is, therefore, given by

$$q_0 = \frac{k_f}{k_f + k_i} \tag{8}$$

where k_f and k_i are the relative probabilities of emission and of quenching, respectively, [9, p. 73–73]. Crystals with high quenching probability will have extremely low luminescence quantum efficiency and, thus, low light yield.

III. COMPUTATIONAL THEORY: MONTE CARLO N-PARTICLE

The method of simulation in this research is the Monte Carlo N-Particle radiation transport code developed at Los Alamos National Lab in Los Alamos, NM. MCNP is described as a "general-purpose, continuous-energy, generalized-geometry, time-dependent" transport code that can be used in several modes to track neutrons, photons, electrons, or various combinations of the three [7]. This chapter will provide a brief discussion of the computational theory and specific features of this code.

A.   MONTE CARLO METHOD

Monte Carlo is a probabilistic approach to simulation that infers a solution by applying random numbers in such a way that they directly simulate physical random processes [12, p. 2]. Therefore, a Monte Carlo calculation is a sequence of random events, each with a distinct probability. In highly complex problems, such as radiation transport, a wide range of factors influence the outcome of random events; these are known as composite events. One example of this complexity is, as the simulation evolves, the code must account for the interdependence of the probabilities of all random events. In such events, assigning a numerical probability to each possible outcome is not useful [13, p. 9–10]. Sophisticated Monte Carlo methods, therefore, introduce random variables which have associated multivariable distributions in order to more accurately characterize the complexity of composite events [12, pp. 10–15]. Probability distributions can be thought of as mathematical descriptions of the dice being rolled in a random event. They encompass the factors influencing the outcome of the event. Monte Carlo methods use the random variables drawn from probability distributions to approximate an integral [12, p 31].

Due to the probabilistic nature of the interaction between radiation and materials, Monte Carlo is an appropriate tool for simulating such events. Unlike deterministic transport methods, which solve a transport equation for the average particle, the Monte Carlo method tracks individual simulated particles from collision to collision and tallies

some aspect of their average behavior [7, p. 1.2]. The random history of each particle is governed by rules (derived from physics) and probability (derived from cross-section data) to determine number, locations, and nature of interactions that occur [6, p. 1.3].

Figure 8 shows the history of a neutron as it passes through a fissionable material. As the incident neutron interacts with the material, particles are created, lost, or scattered at each numbered event. Created particles are recorded, banked, and later tracked through random sampling. All particles are tracked until termination, whether through capture, annihilation, or leakage from the area under investigation.

Event Log

1. Neutron scatter, photon production
2. Fission, photon production
3. Neutron capture
4. Neutron leakage
5. Photon scatter
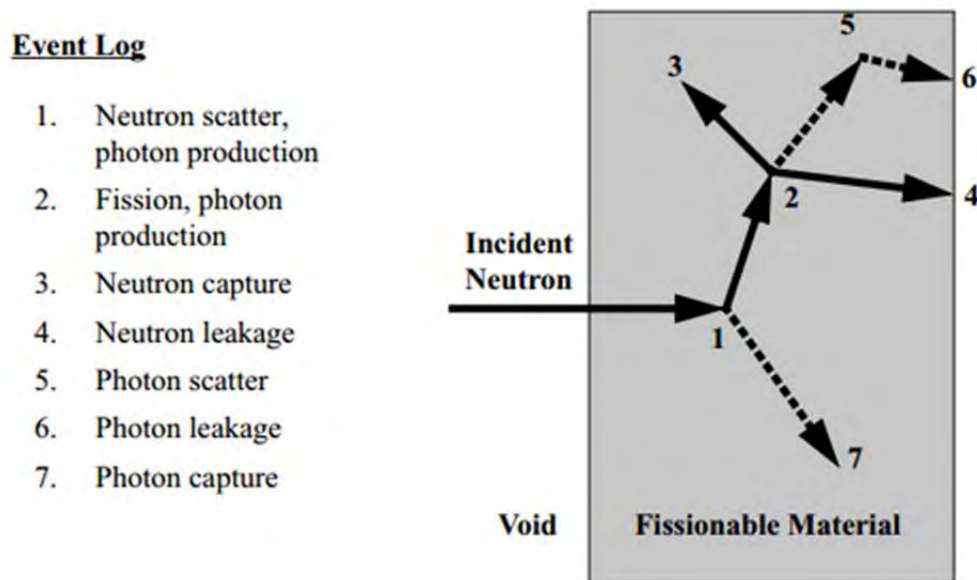6. Photon leakage
7. Photon capture

Figure 8.   MCNP history of neutron incident on fissionable material with numbered events, from [7].

B.   MCNP PHYSICS

The rules and probabilities governing the random histories in MCNP rely on some central concepts and information, including particle weight, particle tracks, and interaction data.

1.   Particle Weight

MCNP models are not exact simulations of physical processes in nature. In each model, a distinct number of particles are generated and simulated starting from the radiation source, but that number does not represent the number of particles present in reality. Rather, one simulated particle in MCNP represents several physical particles all being transported with the same random walk. So a MCNP particle representing w physical particles has an initial weight of w. While is this not a exact simulation, the average statistical behavior of the total number of physical particles is observed by multiplying the results of each simulated particle by its corresponding weight [7, p. 2.25]. There are several benefits of using particle weight. First, calculating less random walks is more computationally efficient. Secondly, having weighted tally contributions in the final results allows users to normalize their calculations to various source strengths. Finally, this technique allows the code to sample areas of interest in the problem without degrading the precision of the results [7, p. 2.25].

2.   Particle Tracks

Particle tracks characterize each component of a source particle during its entire history [7, pp. 2.26]. A track is created for each particle as it leaves the source and keeps a record of its behavior. If the particle undergoes some process that requires an additional track, like a photon undergoing pair production, the track will split into two, each with a half of the original source particle weight. A track can split several times in the history of the source particle, as seen in Figure 8, but the weight of all will sum to the original particle weight. Particle tracks are necessary for making the tally calculations desired by the user. For example, surface estimators use the number of tracks crossing a surface to calculate particle flux.

3.   Data Libraries

Determining the number of collisions experienced by a particle and the nature of those collisions requires the nuclear data tables included in the MCNP code package. The MCNP data libraries are updated with data from U.S. Evaluated Nuclear Data File

(ENDF), which is maintained by the Cross Section Evaluation Working Group (CSEWG). MCNP specifically contains data from the ENDF/B library with some supplemental data from a few other libraries, including the Lawrence Livermore National Laboratory's Evaluated Nuclear Data Library (ENDL) [7, p. 2.16]. There are 9 classes of data tables for MCNP, including continuous-energy neutron interaction data, discrete reaction neutron interaction data, continuous-energy photoatomic interaction data, and electron interaction data [7, p. 2.14].

C.   TALLIES

All MCNP simulations automatically give standard summary reports about the physics and reliability of the calculations. That report includes general information about the creation and loss of tracks, particle activity in each cell, particle activity of each nuclide, and particle weight [7, pp. 2.80]. Specific calculations about the behavior of particles, however, require the use of tallies. MCNP tallies keep track of a specific phenomenon throughout the entire simulation and calculated the desired quantity specified by the user. There are seven standard types of tallies, shown in Figure 9, but each can be modified, providing for a large variety of calculations. Two of these tallies are particularly central to this study and are briefly deliberated in this section.

	Tally Mnemonic			Description
F1:N	or F1:P	or	F1:E	Surface current
F2:N	or F2:P	or	F2:E	Surface flux
F4:N	or F4:P	or	F4:E	Track length estimate of cell flux
F5a:N	or F5a:P			Flux at a point or ring detector
F6:N	or F6:P	or	F6:N,P	Track length estimate of energy deposition
F7:N				Track length estimate of fission energy deposition
F8:N	or F8:P	or	F8:E	Pulse height tally
		or	F8:P,E	

Figure 9.   Overview of MCNP tallies with description.

1. Cell Flux Tally (F4)

All space within a MCNP model is inside of user-defined cells, which are delineated by geometric surfaces. The F4 tally uses the track lengths in a cell to calculate the average particle flux in that cell (particles/cm^2). The theoretical integral representing this tally is

$$F4 = \frac{1}{V} \int_{E_i} dE \int_{t_j} dt \int dV \; \phi(\vec{r}, E, t)$$

where V is the cell volume and $\phi(\vec{r}, E, t)$ is the scalar flux for a particular position, energy, and time [7, pp. 2.85]. However, the scalar flux can be thought of as the particle velocity v times the density of particles a point N,

$$\phi(\vec{r}, E, t) = vN(\vec{r}, E, t).$$

Furthermore, defining differential track length to be

$$ds = vdt$$

gives an average particle flux of [7, pp. 2.85–86]

$$\overline{\phi}_V = \frac{1}{V} \int dE \int dV \int ds \; N(\vec{r}, E, t).$$

$N(\vec{r}, E, t)ds$ can be thought of as a track length density, so the entire triple integral is approximated by a weighted sum of all the particle tracks in the cell with volume V.

2. Tally Multiplier Card (FM)

One way to modify an MCNP tally is with a FM card. FM cards convert the quantity of a tally into a value of different units. For example, the user can apply an FM card to convert a neutron flux tally (particles/cm^2) into a calculation of total inelastic scattering events within that cell. FM cards can convert F1, F2, F4, and F5 tallies by multiplying them by continuous-energy data from the cross sections' libraries. The quantity calculated for such modified tallies is

$$C \int \varphi(E) R_m(E) dE,$$

where $\varphi(E)$ is the energy-dependent fluence (particles/cm^2) and $R(E)$ is the continuous-energy response function from the nuclear data tables [7, pp 3.99–101].

3.   Energy Deposition Tally (F6)

The F6 tally is a track length flux tally (F4) modified to tally the amount of energy deposited to the material by the incident particles (MeV/g). Energy deposition calculations can also be done using a F4 tally and with the proper FM card. For each F6 tally, MCNP uses a heating function, H(E), from the data libraries to calculate the amount of energy released during particle collisions. The heating function for neutron radiation is defined as

$$H(E) = E - \sum_i p_i(\mathrm{E})[\bar{E}_{i,out}(E) - Q_i + \bar{E}_{i,\gamma}(E)],$$

where $p_i(E)$ is the energy-dependent probability of reaction i, $\bar{E}_{i,out}(E)$ is average exiting neutron energy, Q_i is the Q-value for the reaction, and $\bar{E}_{i,\gamma}(E)$ is the average exiting gamma energy for the reaction [7, pp. 1.87–89]. The index i iterates over all possible neutron interactions for each collision. The heating function for photons has a similar structure, where i iterates over Compton scattering, pair production, and photoelectric absorption.

IV.   GAMMA RADIATION

Because fissile materials are sources of both neutrons and gamma rays, increased detection sensitivity for such material can be achieved by systems that can detect both forms of radiation [14]. Therefore, the initial investigation of the crystal set aims at getting a more robust understanding of the gamma-crystal interactions discussed previously in this paper (seen in Figure 10). Previous and ongoing experimental study in this area includes optical characterization, cathodoluminescence characterization, and gamma-induced scintillation. The following is the section is meant complement those efforts from a computational approach.
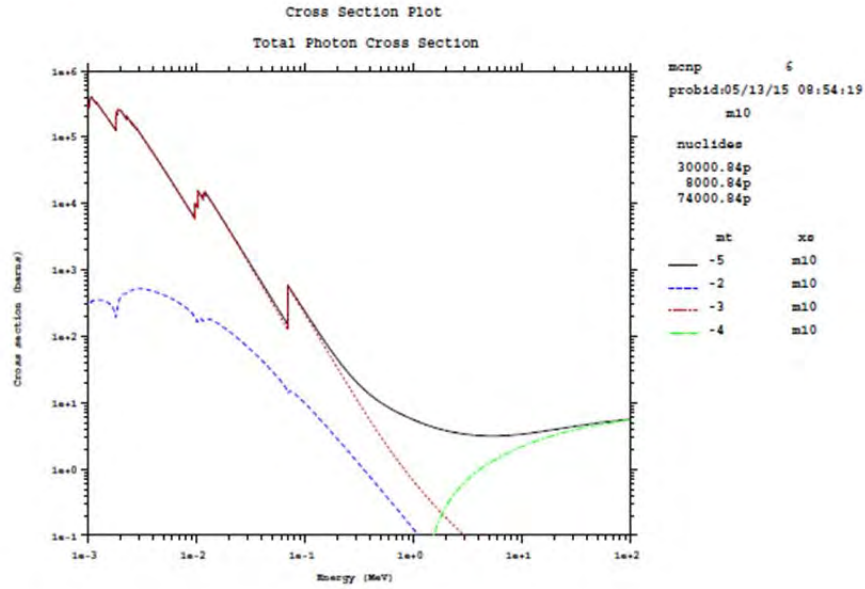
Figure 10.   MCNP Cross Section plot of photon cross sections for ZWO: -5 is total cross section, -2 is Compton scatter, -3 is photoelectric abs., and -4 is pair production.

A.   INTERACTIONS

As discussed in the background physics chapter, the three main interactions gamma rays have with matter are pair production, photoelectric absorption, and Compton scatter. An F4 tally with a reaction multiplier card was used to calculate different

23

interactions that take place when each of the six different crystals (listed in Chapter I) is exposed to gamma radiation. Overall, there were very little differences of interactions between all of the crystal. As expected, photoelectric absorption dominated the left side of the energy spectrum, especially for energies less than 0.5 MeV. Compton scattering dominated the middle part of the energy spectrum between 0.5 and about 4–5 MeV. In all the crystals except YSO, pair production became significant at around 2 MeV, as indicated by the ZWO cross sections plot in Figure 10 and shown in the simulated ZWO interactions in Figure 12(a) (which is representative of the other five crystals). Only YSO deviates from this norm, showing a more gradual rise of pair production at about 4.2 MeV (Figure 12(b)). All crystals exhibited an exponential decay of total interactions with increasing energy. There was little deviation from total number of interaction for all the crystals except YSO, which showed about 40% less total number of interactions, as shown in Figure 11. This is most strongly influenced by the fact that the density of YSO is roughly 40% lower than the average density of the other 6 crystals under study.
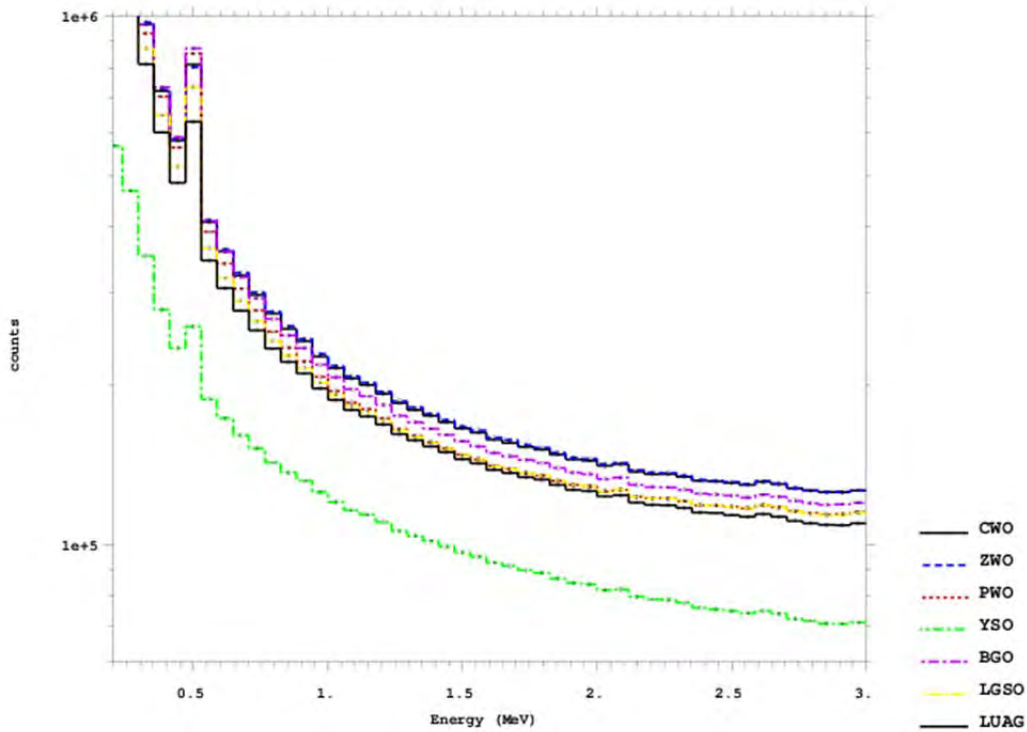
Figure 11.   Total number of reactions against energy of incident gamma radiation
for each crystal.
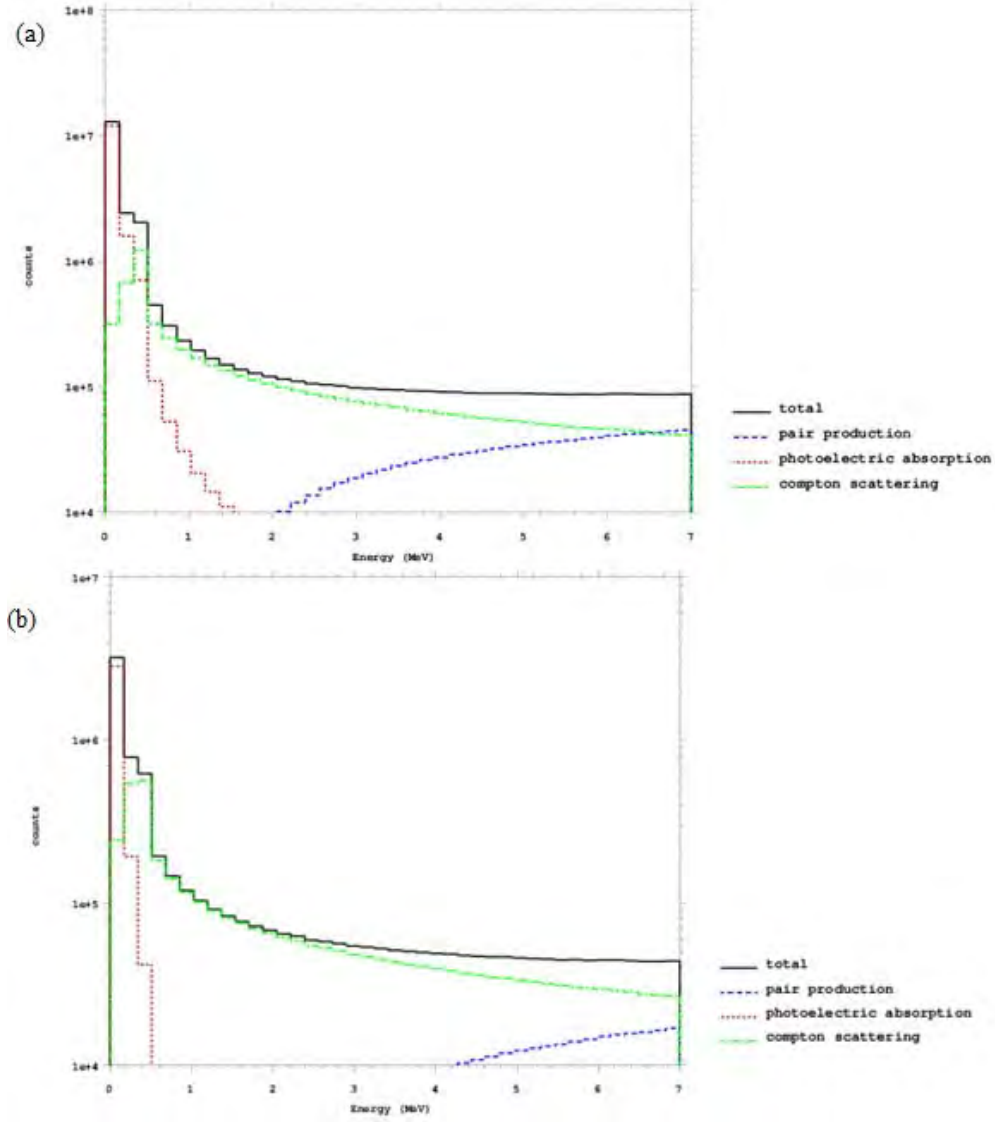
Figure 12.   (a) ZWO reactions from incident gamma spectrum.
(b) YSO reactions from incident gamma spectrum.

B.   ENERGY DEPOSITION

An energy deposition tally (F6) was used to see how energy deposition was related to specific crystals, interaction types, and incident gamma energy. Initially, a flat distribution of gamma emissions from 0 to 7 MeV was used, meaning gamma quanta of all energies in that range were equiprobable. This would allow any crystal-specific characteristics that might affect energy deposition to be readily identifiable. The only

such prominent distinction was a roughly 40% decreases in energy deposition for YSO (shown in Figure 13), which is most probably a result of 40% lower density.
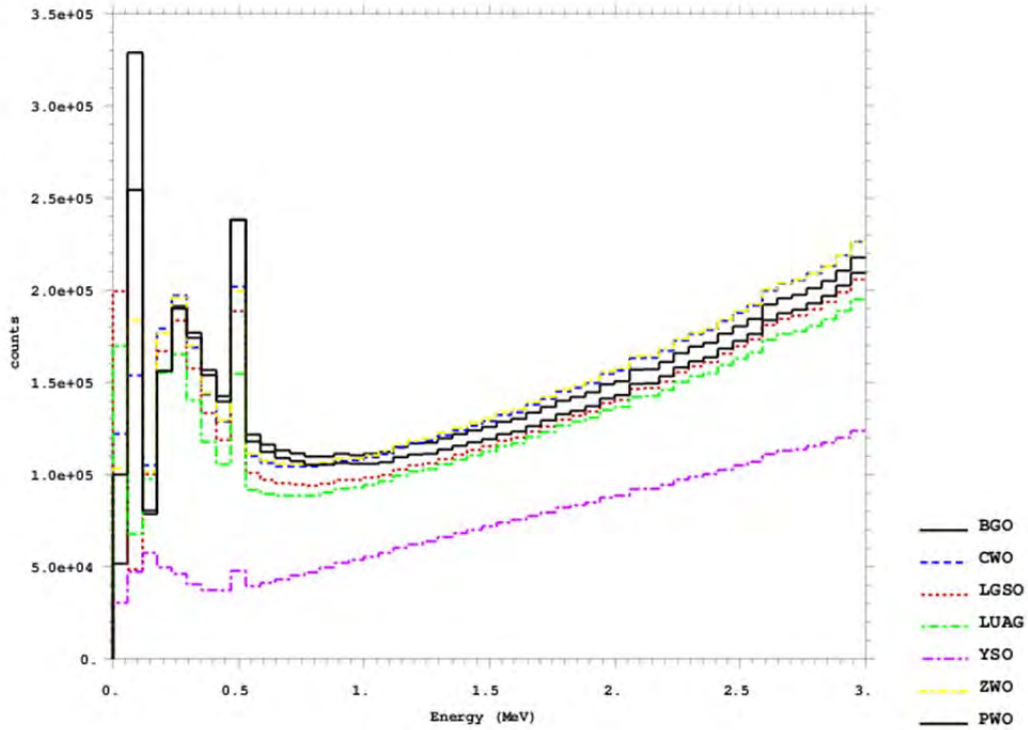
Figure 13.   Total energy deposited to each crystal vs. incident gamma energy.

Comparing Figures 11 and 13 gives an indication what which interactions deposit the most energy into the scintillator. Compton scatter makes up the largest percentage of gamma interactions in each of these crystals, especially in the middle spectrum of 1–4 MeV. The largest energy deposits, however, occur at energies less than 0.7 MeV and greater than 2 MeV, which are dominated by photoelectric absorption and pair production, respectively.

Simulation of the energy deposition in a gamma-induced scintillation experiment was also done [15]. For each crystal, the optical emissions were measured during a 180-second time interval while exposed to Cobalt 60 and Barium 133 (specifications in Table 3). The source was placed directly against the crystal for each measurement. The half-life, initial activity, and date of manufacture for each source were used to calculate

the number of gamma emissions released at the time of the measurements in 180 seconds. The results of the energy deposition calculations for each crystal and each source are shown in Table 4. The goal is to acquire photon emission in this setup in photons per second for each crystal and divide it by energy deposition over the 180 seconds to get the absolute light yield in photons per MeV for each crystal. This is an ongoing effort and additional measurements will be are needed to accomplish this in the following weeks.

Table 3.   Specifications of cobalt and barium sources used in crystal measurements at NPS.

	Co-60	Ba-133
Original Activity	1 μCi	1 μCi
Half-life (yrs.)	5.27	10.8
Energy (MeV)	1.173, 1.333	0.081, 0.276, 0.303, 0.356, 0.384
Date of manufacture	October 2006	October 2007

Table 4.   Energy deposition calculations for simulation of gamma induced scintillation, from [15].

crystal	Co-60 Energy Dep. [MeV]	Ba-133 Energy Dep. [MeV]	density [g/cm^3]
BGO	1.58E+05	1.54E+05	7.13
CWO	1.56E+05	1.37E+05	7.9
LGSO:Ce	1.40E+05	1.34E+05	7
LUAG:Ce	1.34E+05	1.21E+05	6.73
PWO	7.65E+05	2.32E+05	8.28
YSO:Ce	7.62E+04	4.09E+04	4.44
ZWO	1.57E+05	1.38E+05	7.87

THIS PAGE INTENTIONALLY LEFT BLANK

V. NEUTRON RADIATION

The proposed detection method hinges on internal counting of gamma quanta in the energy of range of 10–1000 keV produced as a result of inelastic scattering by heavy nuclides in the crystal material [14]. This research is based on the assumption that inelastic scattering must be a significant portion of neutron-crystal interactions (seen in Figure 14). This section uses MCNP to investigate those interactions.
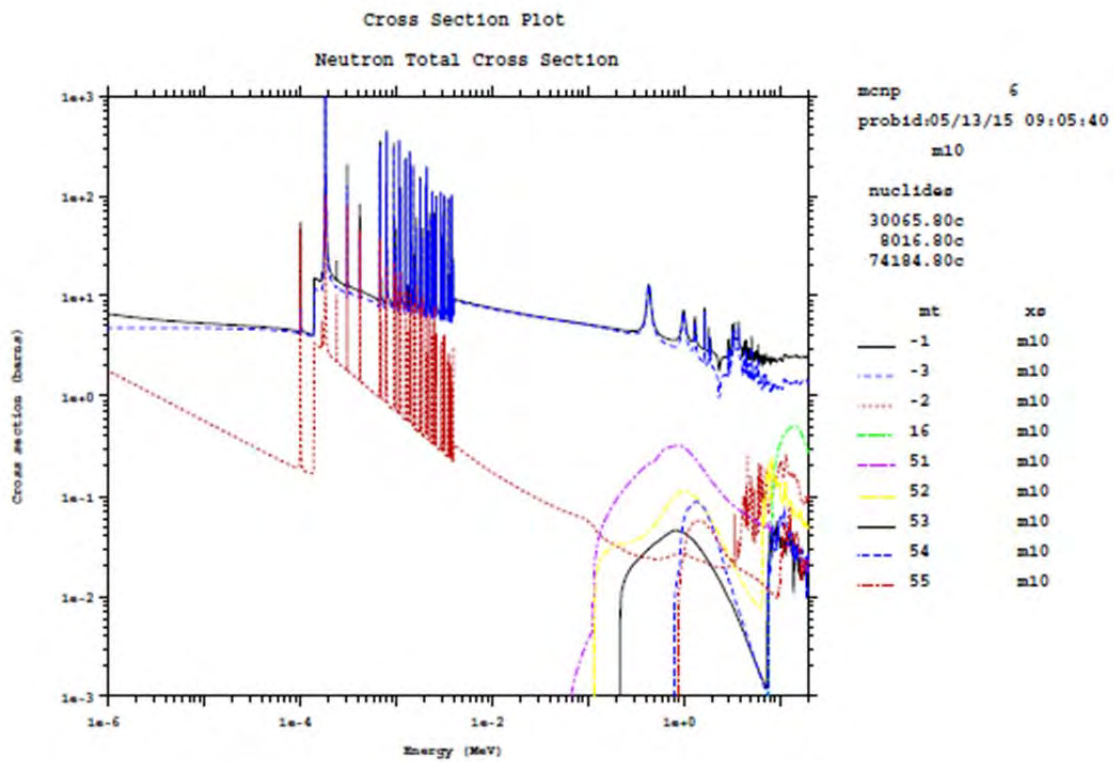

Figure 14.   MCNP cross section plot for ZWO. -1 is total cross section,
-3 is elastic scatter, -2 is absorption, 16 is fission, and
51–55 are inelastic scatter.

A.   INTERACTIONS

A track length flux tally (F4) with multiplier cards was used to better understand the reactions inside the crystal set. The multiplier cards indicate the desired neutron

interactions with the chosen material, as shown for the neutron cross section plot for ZWO in Figure 14. Notice that elastic scattering accounts for a large percentage (>75%) of the total cross section for ZWO at energies below 1 MeV. It is also important to note that inelastic scattering only becomes appreciable at around 1 MeV. The total inelastic cross section is actually the sum of several individual inelastic cross sections for each excited state for a specific nuclide. In Figure 14, cross sections 51–55 are all inelastic scattering.
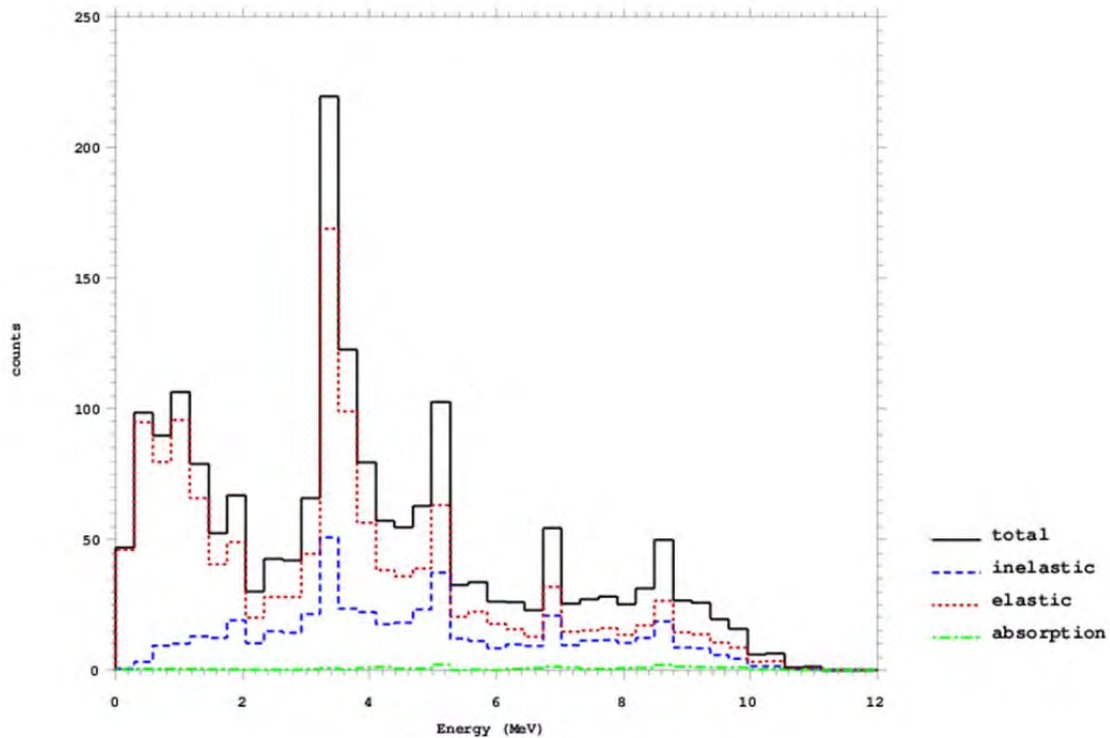
Figure 15.   Neutron interactions from PuBe source incident on CWO.

The interactions of neutrons emitted by a PuBe source in CWO are shown in Figure 15, which is fairly representative of the crystal set (shown below). For each set, elastic scattering makes up about 75–85% of the total interactions depending on the crystal. Absorption (green curve in Figure 15) does not make up an appreciable percentage of the neutron interaction with the given crystals and fission does not occur for these materials. Inelastic scatter makes up about 15–25% of the total neutron interactions, depending on the crystal. This is in agreement with the inelastic cross

section plot discussed in the background physics chapter. From the plot of total inelastic scattering for each crystal (Figure 16), little variation in the spread of inelastic scattering across the energy spectrum is seen.
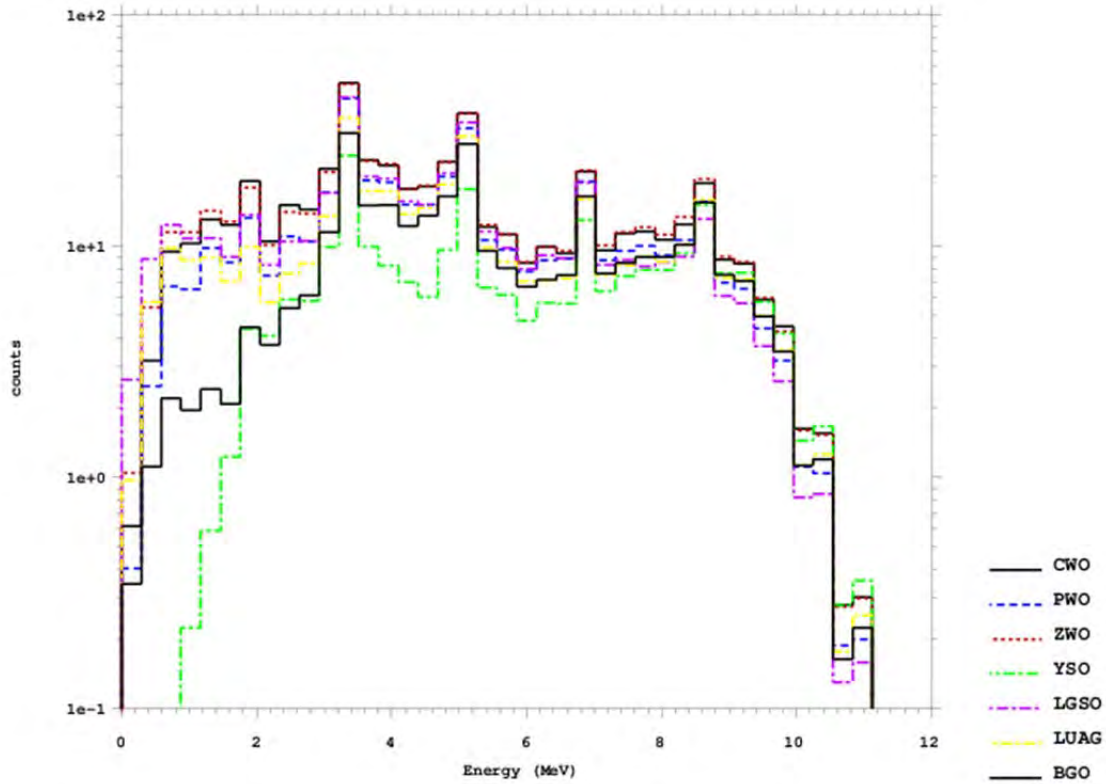
Figure 16.   Inelastic scatter of each crystal against neutron energy.
Lower black line is BGO.

The biggest deviations from the norm are BGO (lower black line) and YSO:Ce, which seem be less likely to experience inelastic scatter at energies below 3.5 MeV. YSO overall has fewer interactions than the rest of the set, which includes inelastic scattering.

B.   DETECTION EFFICIENCY

The detectable radiation-matter interactions in a scintillator produce photons which are transformed into recordable pulses. If every neutron that enters a crystal medium results in a detectable signal, the detection system has 100% neutron counting

31

efficiency [10]. Therefore, for the purposes of this study, detection efficiency will be defined as the ratio of recorded pulses to the number of radiation quanta incident on crystal medium. All MCNP investigations of detection efficiency in this thesis (plotted in Figures 17 and 18) make the assumption that each neutron or gamma collision with the scintillator crystal results in a detectable signal (i.e., a recorded pulse), and should, therefore, be interpreted as an upper-limited of achievable counting efficiency for a detection system with this set of candidate crystals. Similarly, detection efficiency based on specific interaction actions, such as inelastic scattering, is also investigated.
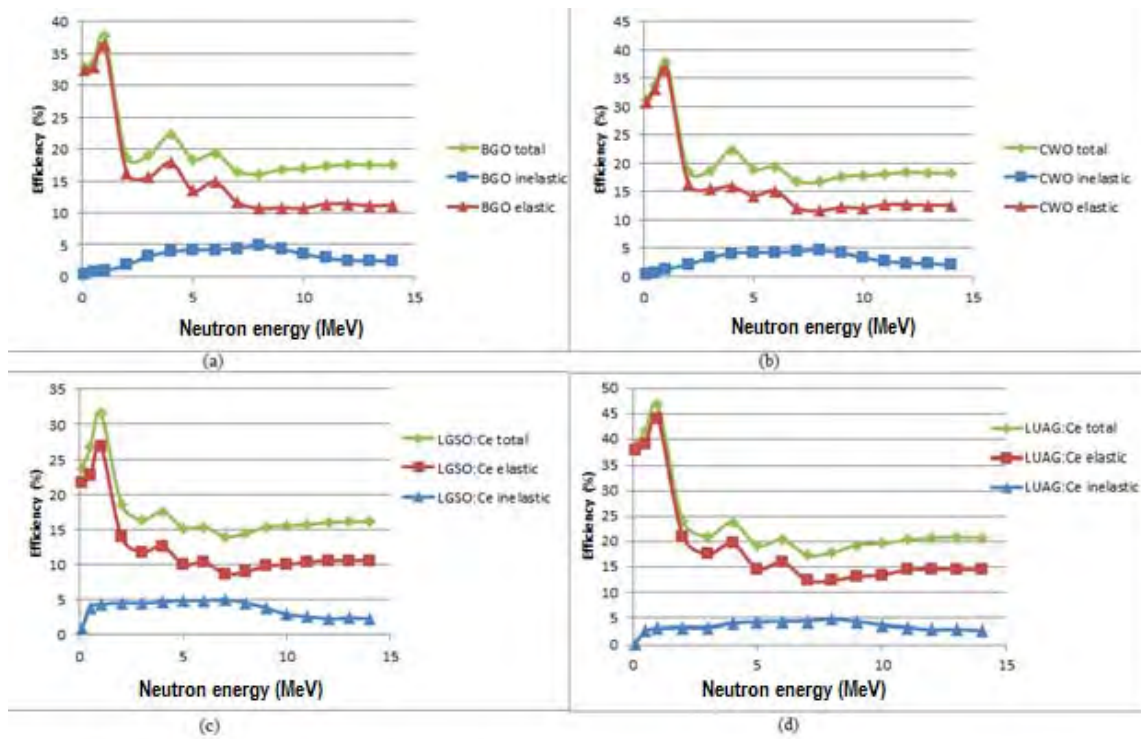
Figure 17.   Response curves for (a) BGO, (b) CWO, (c) LGSO:Ce, and
(d) LUAG:Ce based on the upper limit of detection efficiency
discussed above.

The response curves shown in Figures 17 and 18 were calculated by dividing the total number of neutrons that experienced a reaction by the total number of neutrons entering the crystal medium. The elastic (red) and inelastic (blue) curves represent the ratio of total number of neutrons with that specific interaction to the total neutrons

entering the crystal. The curves reveal that elastic scattering accounts for almost all of the interactions taking place at less than 1 MeV. This is in agreement with the neutron cross section plots, as discussed earlier. For most of the crystal, inelastic scattering rises significantly around 1 MeV and falls off around 10 MeV. YSO is an exception to this as that curve does not begin to drop off until around 12–13 MeV. All tungstate crystals have a prominent plateau from about 2-8 MeV. Both crystals containing Lutetium (Lu) have sharp rises in inelastic scattering at very low energies.
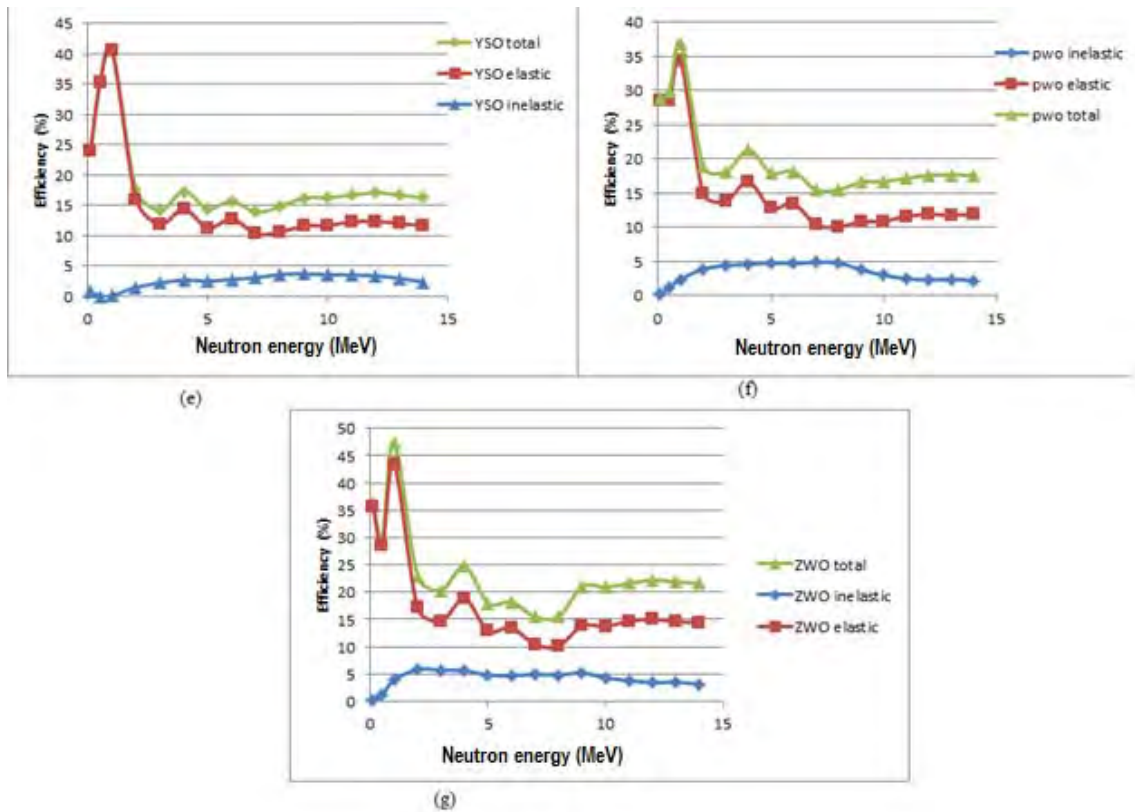

Figure 18. Response curves for (e) YSO, (f) PWO, and (g) ZWO based on the upper limit of detection efficiency discussed above.

THIS PAGE INTENTIONALLY LEFT BLANK

VI.   DETECTOR MODEL

A MCNP model of the detector configuration used in experimental investigation of the crystals was built and used to assess the achievable fast neutron detection efficiency for the candidate set of crystals. The experimental setup (shown in Figure 19) consists of (1) Pu-Be fast neutron source, (2) 10mm x 10mm x 10 mm scintillator crystal, (3) R1306 type PMT, (4) gadolinium oxide cylindrical absorber surrounding the crystal with thickness of 10 mm, (5) gadolinium oxide lid of cylindrical absorber, (6) lead shielding of 40 mm thickness, and (7) lead protection surrounding the source of 4 mm thickness. The middle 40 mm thick lead shield (6) and the 4 mm lead shield around the source (7) both served as protection from the contaminant gamma radiation from the neutron source that could interference with neutron detection [14]. Various components of the configuration were studied, as well as the effectiveness of the experimental setup as a whole. In all simulations, the distance between the Pu-Be source and the scintillator crystal was held constant at 200 mm, while other components of the configuration were varied.

Figure 19.   Basic experimental set up for crystal experiments in NASU.

A.   SUPPRESSION OF BACKGROUND GAMMA RADIATION

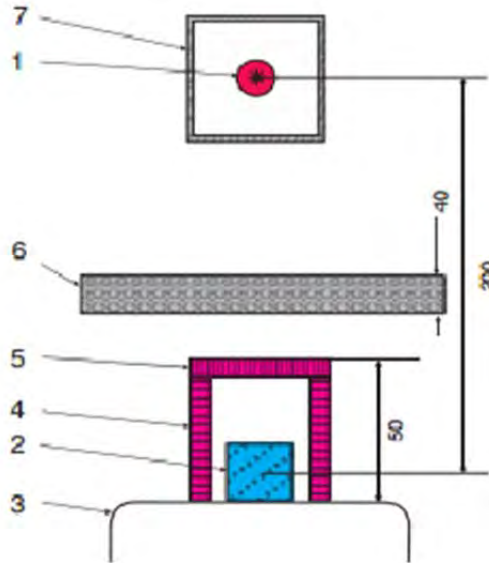Experimental efforts to suppress background radiation were simulated using MCNP. In addition to neutron radiation, Pu-Be and other neutron sources emit gamma radiation. The gamma spectra from Pu-Be is specifically a result the following nuclide reactions:

$$^{241}Pu \rightarrow {}^{241}Am \rightarrow {}^{237}Np \tag{9}$$

$$^{9}Be \rightarrow {}^{4}He \rightarrow {}^{12}C^{*} + n \tag{10}$$

$$^{9}Be \rightarrow {}^{4}He \rightarrow {}^{13}C^{*} \tag{11}$$

$$^{10}Be\left(n,\gamma\right){}^{10}Be^{*} , \tag{12}$$

which emit 59.54 keV, 4.43 MeV, 3.68 MeV, and 3.37 MeV gamma quanta, respectively [14]. Gamma radiation accompanying neutrons can severely interfere with neutron detection because there is no way to differentiate between gamma quanta that result from neutron interactions in the crystal and contaminant gamma radiation emitted by the neutron source. The goal was to shield the scintillator from contaminant gamma flux in the energy range of 30–300 keV without significant shielding of the incoming neutron radiation from the Pu-Be source. Previous study has shown experimentally that this gamma-background can be sufficient suppressed through passive protection with lead shielding [24]. It was shown that suppression of background gamma radiation by a factor of 10^{3} could be achieved in the working range of 30–300 keV [14].

A simulation of the experiment verified the effectiveness of Pb shielding for the suppression of contaminant gamma-background by calculating the energy deposited to the crystal at different thickness of Pb shielding. The energy range and Pb shield thicknesses investigated were identical to the original study. However, an equiprobable distribution of gamma ray emissions in the energy range of 0.3–900 keV was used instead of the Pu-Be gamma spectrum. This gave a more complete description of the effectiveness of shielding at different energies. Simulation showed that 54 mm of Pb shielded the crystal from virtually all gamma radiation, which agrees with previous experiment.
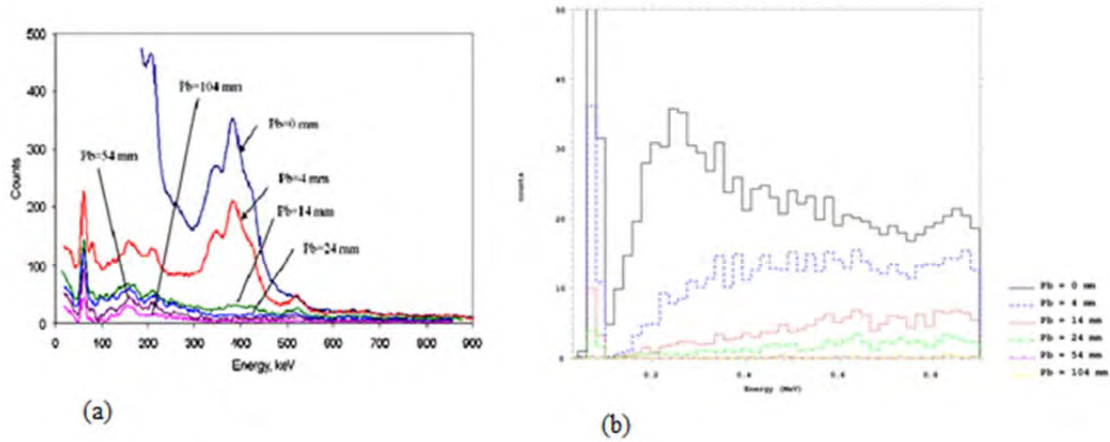
Figure 20.   (a) Experimental measurements of CWO with low energy PuBe
gamma spectra with different Pb shield thicknesses. (b) MCNP energy
deposition calculations in CWO with flat distribution of gamma
in equivalent energy range.

A shielding thickness of 40 mm was selected as the optimal thickness for minimizing gamma quanta in the relevant energy range without significantly suppressing neutron flux. Indeed, simulation showed (in Figure 21) 40 mm Pb shield decreased background-gamma energy deposition by almost 100% while only reducing energy deposition from neutrons by about 18%. However, 54 mm of Pb reduces the neutron energy deposition by almost 30%.

37

Figure 21.　(a) CWO energy deposition from gamma radiation in 0-900 keV with Pb shield thickness of 0 mm (black) and 40 mm (blue). (b) CWO energy deposition from PuBe neutron source in energy range from 0–12 MeV with Pb shields of 0 mm (black) and 40 mm (blue).

B. MODERATION

Proposed moderation techniques were also investigated using MCNP. The two configurations studied are shown in Figure 22. Figure 22 (a) is identical the basic experimental setup described above, except without the gadolinium oxide lid, which was used as a ther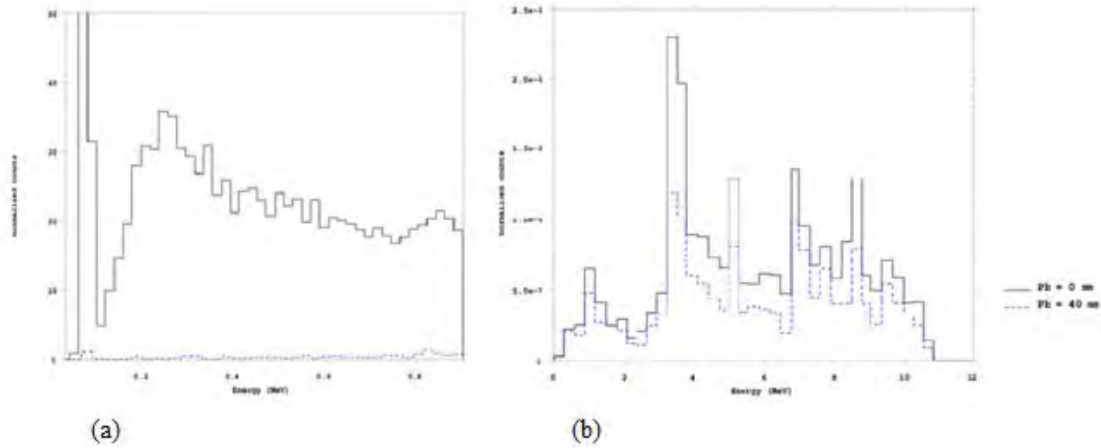mal neutron absorber. Figure 22 (b) includes the gadolinium oxide lid (5) along with a polyethylene moderating cylinder of 65 mm thickness (8) surrounding the PuBe source. The effects of the moderating elements can be seen by looking at the energy deposited to the crystal with and without those elements. The function of a moderator is to bring down the energy of an incident particle in order to make conditions more suitable for a desired reaction, like neutron absorption.

The desired effect for this detector configuration is achieved and is demonstrated, to a degree, in the energy deposition results in Figure 23. For all energies above 3 MeV, the energy deposited to the crystal was noticeably less for the moderated configuration. However, the moderated setup resulted in high energy deposition for energies below 2.6 MeV. From this process of bringing higher energy neutrons to lower energy neutrons, it is reasonable to infer that a percentage of higher energy neutrons that would likely pass

through the crystal without interaction would be brought to energies more optimal for interaction with the use of this moderation configuration.
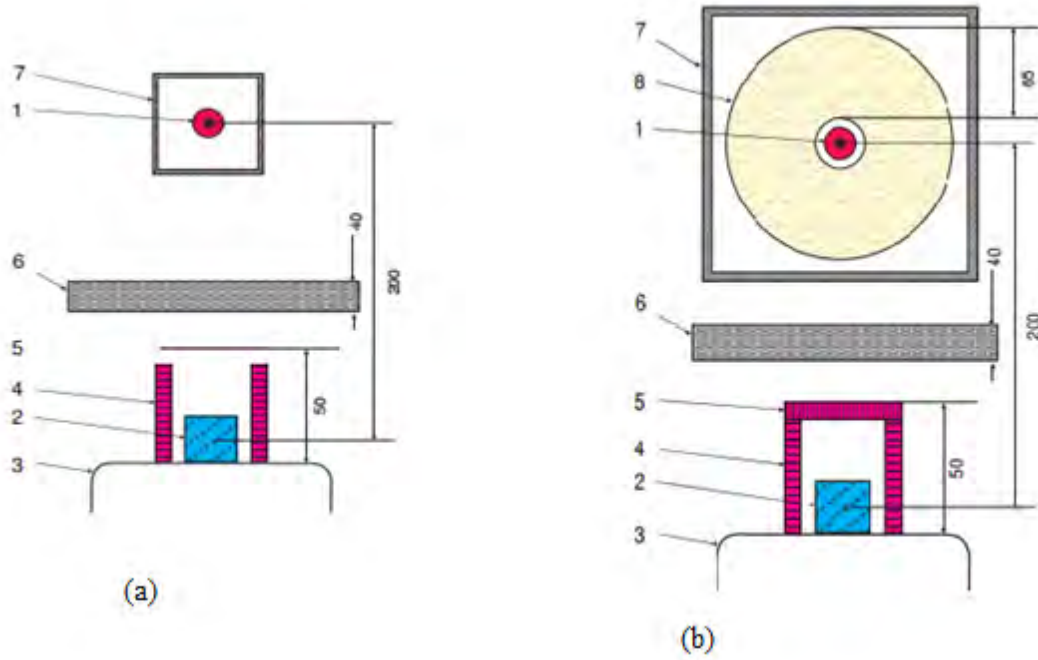
Figure 22.   (a) experimental setup without moderation. (b) experimental setup with 8–polyethylene moderator around source and 5–gadolinium oxide lid.
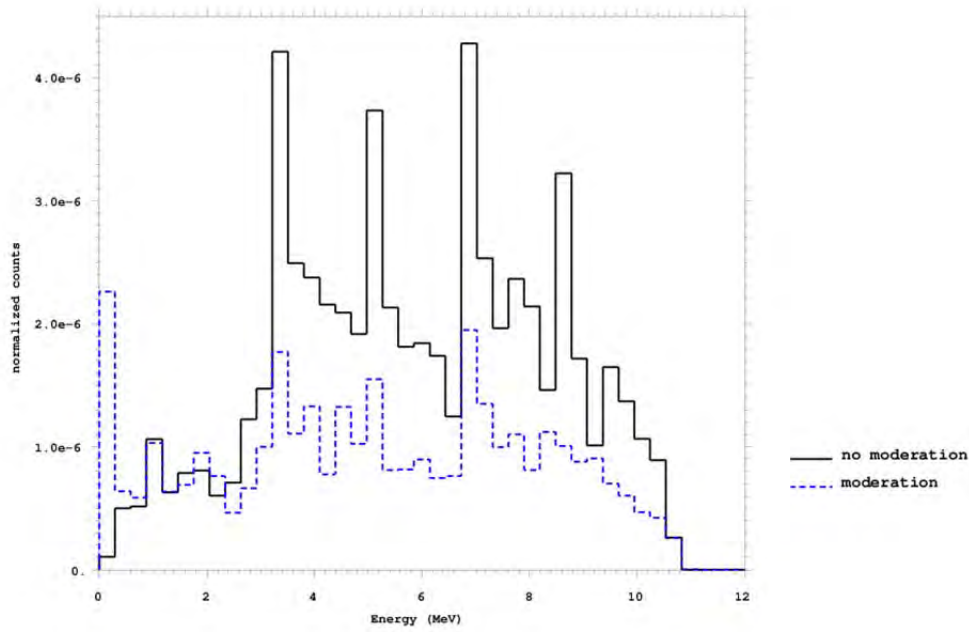
Figure 23.   Energy deposition in CWO by PuBe neutrons with (blue) and
without (black) moderation.

Previous experiment with with a slightly different set of crystals determined fast neutron detection efficiency through internal counting of gamma-quanta that result from inelastic scattering (n,n'γ) with energies of 10–1000 keV [14]. Results (Figure 24) reported a linearly dependent relationship between detection efficiency and effective atomic number of the scintillator crystal. The study also showed a steeper trend of increasing detection efficiency of fast and slow neutrons with effective atomic number than with that of only fast neutrons, indicating their moderation technique was more effective with crystals of higher Zeff. Those experiments indicated detection efficiencies of both fast and slow neutrons up to 70–80%.
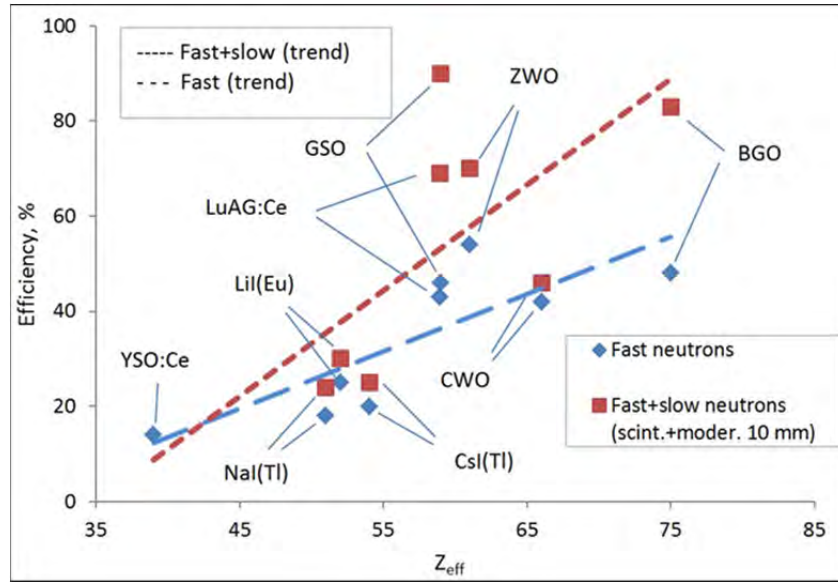
Figure 24.   Detection efficiency of fast and thermal neutron from fluxes from
PuBe source measured by inelastic scattering at ISM,
Ukraine, from [14].

Simulation of the crystals in this study, along with NaI:Ti, CsI:Ti, LiI:Eu, and GSO for completeness, showed a similar increases in detection efficiency with effective atomic number (Figure 25). The model also showed an overall increase of detection efficiency with the moderated configuration, as seen in experiments. Simulated efficiency plotted against the product of Zeff and crystal density (Figure 26) revealed a slightly more linear relationship, which indicates a significant contribution of crystal density to detection efficiency.
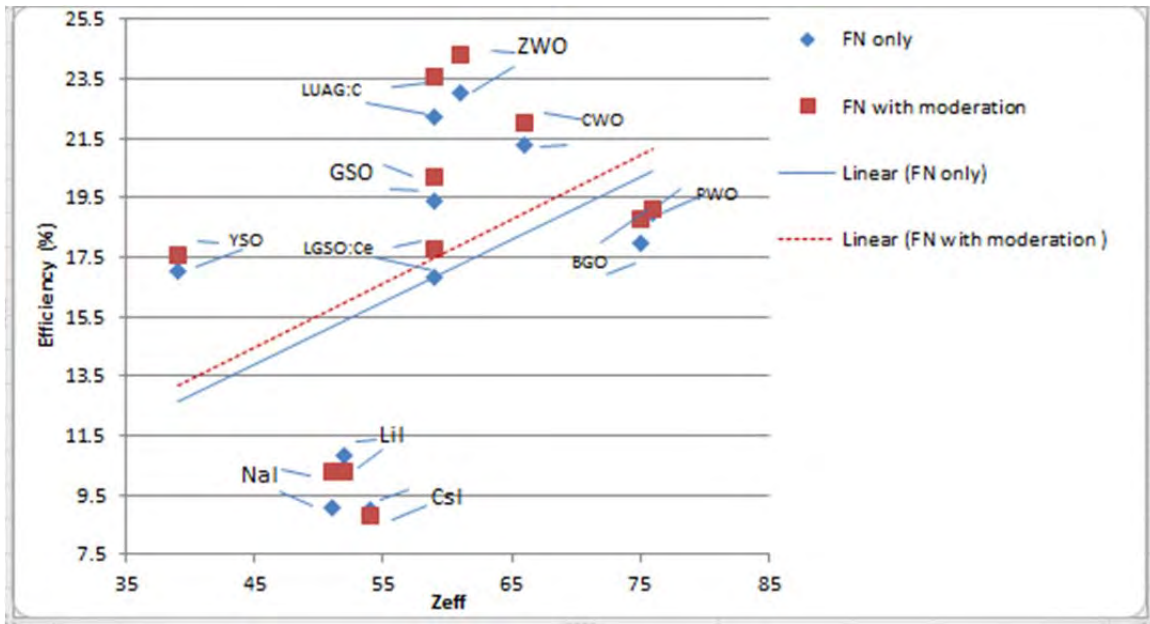
Figure 25. MCNP approximation of detection efficiency for several inorganic
scintillator crystals with (red) and without (blue) moderation.

However, the significant increase in slope of the fast and slow neutron detection efficiency trend was not seen in this model. Neither did detection of fast and thermal neutron go above 25% for the configurations proposed. A contributing factor to these discrepancies could be differences in exact moderator density or geometry. Diagrams of experimental setups were followed closely in the creation of the MCNP model geometry. However, these details, and others, were not listed, which leaves room for deviation from the original configuration.
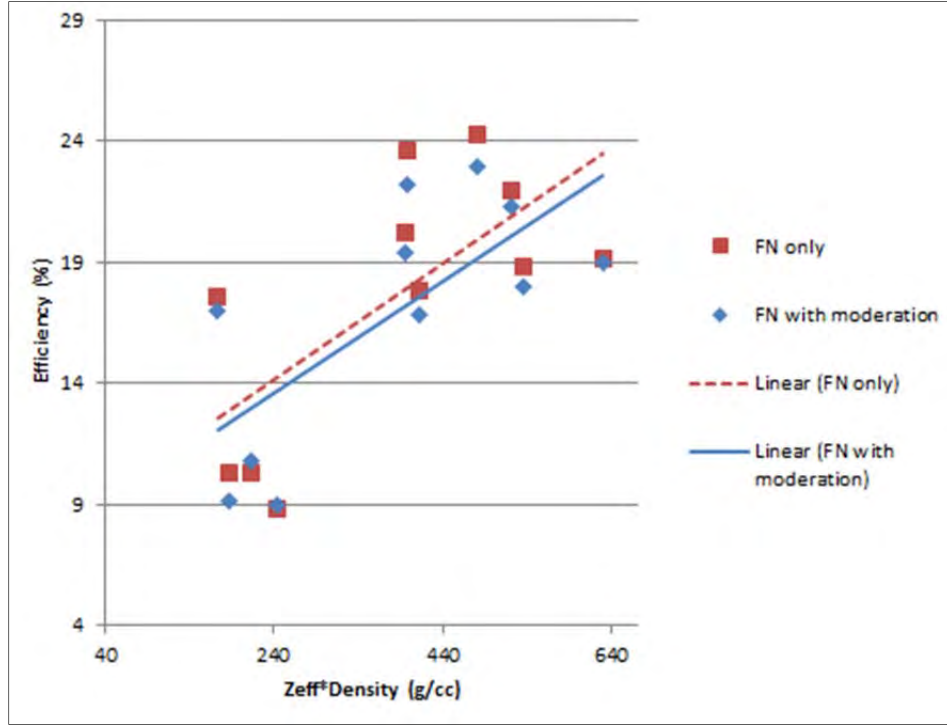
Figure 26.   Calculated efficiency vs. effective atomic number
times density in g/cc.

C.   WHOLE SYSTEM

The basic detector configuration (shown in Figure 19) was modeled and assessed. The model used only neutrons from a PuBe source of 77% Pu-239 in the energy range 0-14 MeV [16]. All crystals had similar behavior for this energy range. BGO demonstrated the high detection efficiency for all energies, except below 1 MeV, where CWO was the highest (plotted in Figure 27). This agrees with the inelastic scattering interactions seen by these crystals in earlier sections of this paper.
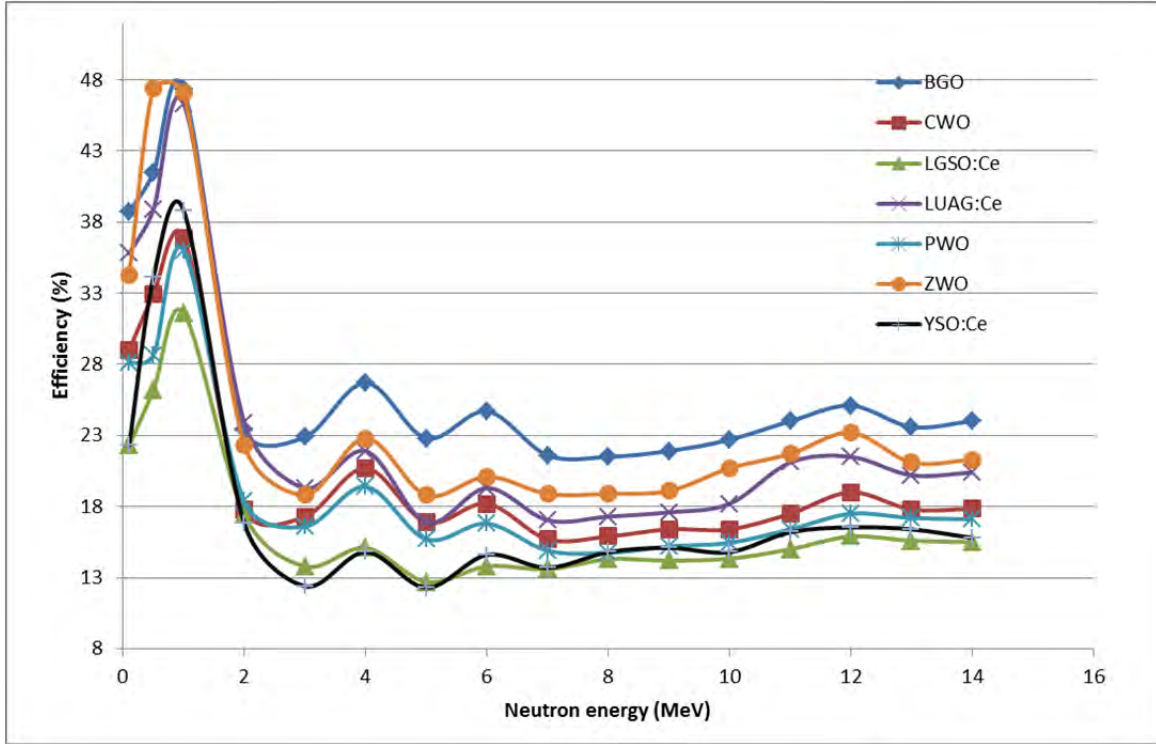
Figure 27.   Response function of basic detector configuration exposed
to PuBe neutron source for each crystal modeled with MCNP.

The significant spike around 1 MeV in the response curve of each crystal accounts for the jump in detection efficiency from fast neutrons only to both fast and slow neutrons that was seen in both experimental and computational study. This underscores the importance of moderation in the configuration to the overall effectiveness of the detection system.

D.   CRYSTAL THICKNESS

Crystal thickness proved to have a heavy influence on the detection efficiency of the crystal set. The potential counting efficiency was approximated, as previously discussed, for a PuBe source incident on a CWO crystal of different thicknesses but constant width and height dimensions. The results are plotted with the inelastic and elastic scatter break down and experimental values (shown in Figure 28). Both simulated and experimental data behave similarly in logarithmic growth with crystal thickness up to

about 4 cm. The measured efficiency, however, remains roughly constant after 4 cm while calculated values continue to grow with decreasing slope.
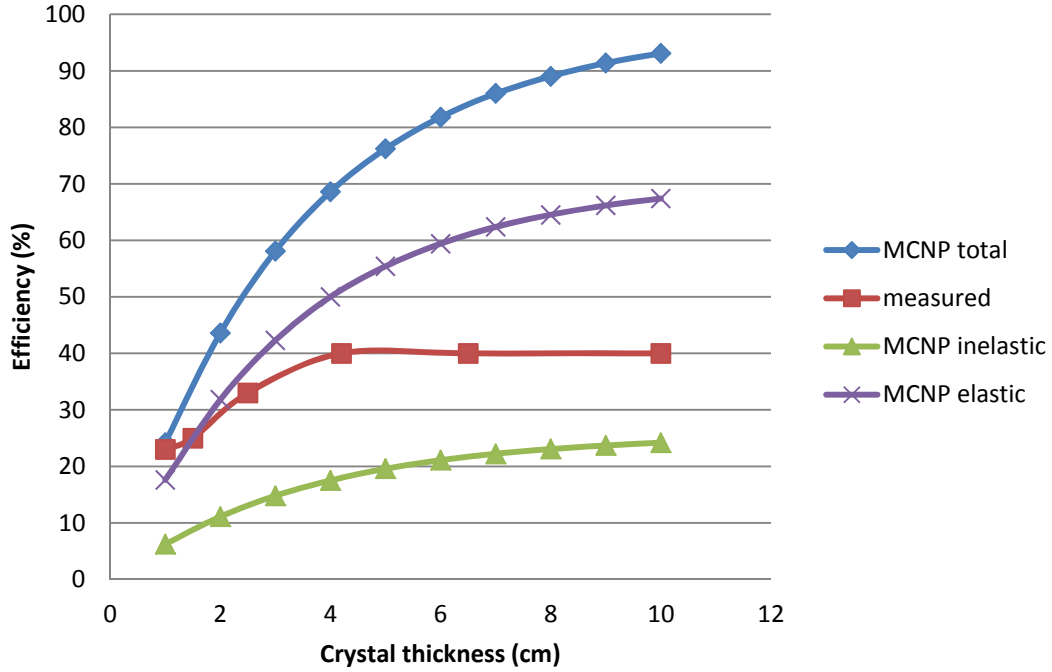
Figure 28.   Measured detection efficiency with calculated efficiency of total interactions, elastic scattering, and inelastic scattering in CWO with increasing crystal thickness.

Further investigation is required to provide a substantial explanation. However, one possible explanation is as follows. Conventional fast neutron detection relies on elastic scattering of neutrons and records resulting gamma quanta using a spectrometric circuit in the energy range above 3 MeV (to avoid interference from background gamma radiation from the neutron source) [5]. In the investigation of this novel method of neutron detection based on inelastic scattering, however, the working energy range of photon detection in these experiments was selected to be 0.02 to 0.3 MeV. This method of internal gamma counting as a form of neutron detection relies on the assumption that 80% of the absorbed neutron flux energy is reemitted in the form of gamma radiation [5]. This seems, to some extent, a reliable assumption for a certain range of crystal thicknesses, based on the logarithmic dependence of efficiency up to about 4 cm (for

CWO). This may not be the case for inelastic scattering of high energy neutrons that are only likely to interact with the crystal when traveling through a thick layer of the medium. If that is true, the photon detection window may be missing the gamma quanta emitted in such high energy collisions.

To further demonstrate the effect of scintillator dimensions, detection efficiency of the proposed detection system with different crystal volumes was calculated and tabulated alongside of measured values (shown in Table 5).

Table 5.   Detection efficiency approximations at different crystal volumes, alongside experimental results. *Some crystals were not tested.

Crystal	Efficiency % (1 cm x 1 cm)	Efficiency % (2 cm x 2 cm)	Efficiency % (3 cm x 3 cm)	Experimental Eff. %
BGO	18.8	35.4	54.5	83
CWO	21.3	42.6	65.2	46
LGSO:Ce	17.2	33.2	51.4	*
LUAG:Ce	22.5	45	57.2	69
PWO	19.2	37.4	57.5	*
YSO:Ce	17.6	34.1	52.2	*
ZWO	23.6	47.5	71.7	70

VII. CONCLUSIONS

The candidate set of heavy oxide and alkali halide crystals have been investigated for potential use in neutron and gamma radiation detection systems. Specific experiments have been modeled with MCNP in a collaborative effort to gain a better understanding of the underlying physics relevant to each configuration. The data presented in this thesis addressed the following research objectives.

1. What radiation-matter interactions occur inside the crystals?

A computational study of the crystal set helped develop a more complete characterization of radiation interactions from both gamma and neutron sources. For incident gamma rays, photoelectric effect dominated below 1 MeV, as expected for these crystals comprised of heavy nuclei, and resulted in a significant spike in energy deposition at energies below 0.7 MeV. Pair production also showed a prominent increased in overall number of interactions and energy deposition above 2–3 MeV depending on crystal. A key takeaway from this study was that all crystals demonstrated very similar behavior when exposed to gamma radiation of energies below 7 MeV, except for YSO:Ce. YSO:Ce had significantly (~40%) less total number of reactions and energy deposition from the rest of the crystals, probably due to its significantly lower density (about 40% less than the average density of the other six).

When neutrons emitted by a Pu-Be source interacted with these crystals, they did so via inelastic scattering 15–27% of the time for the energy range 0–12 MeV. LGSO:Ce demonstrated a particularly high percentage of inelastic scattering at almost 28%, while interactions in the other crystals were closer to 20% inelastic scatter. The other 73–85% of neutron interactions in these crystals was mostly elastic scattering. Neutron absorption and interactions resulting in fission did not comprise a significant portion of the total reactions for this energy range.

2. Calculate energy deposition.

Energy deposited into the crystals by Co-60 and Ba-133 gamma source for each crystal in 180 seconds was calculated and tabulated (see Table 4). This was a simulation

47

of gamma-induced scintillation experiments done at NPS. The goal for these energy deposition calculations was to better characterize the physical properties of the crystals. One component of achieving this was combining the energy deposition calculations with optical output measurements to get the absolute light yield (in photons/MeV) for each crystal. This effort is in process and is expected to be completed in the following weeks.

3. What components of the proposed detection system optimize detection efficiency of a mixed gamma-neutron radiation source?

A model of the proposed scintillator detection system was created and assessed. Various components were investigated as they applied to the overall effectiveness of the detector. The method of background gamma ray suppression in the range of 30–300 keV through the use of Pb shielding of 40 mm thickness was validated. The effects of the proposed moderators were demonstrated in the shift in energy deposition from higher to lower energies and an overall increase in detection efficiency. The increase in the slope of detection efficiency in the moderated configuration against effective atomic number was not seen, however. Further investigation is required. Crystal thickness was shown to strongly increased detection efficiency. The projected logarithmic growth of detection efficiency with crystal thickness was in agreement MCNP approximations, but explanation of the leveling out of measured efficiency after 4 cm requires additional research.

4. What detection efficiency is possible for each of these crystals?

For each configuration, an estimate of the potential intrinsic efficiency was calculated, which can be thought of as an upper limit to the achievable intrinsic counting efficiency for each crystal. With the proposed experimental setup drawn from diagrams, detection efficiency for neutrons emitted from a PuBe source only reached 17–24%, while experimental data suggested detection efficiencies no less than 40%.

There are several factors that could be contributing to this discrepancy. First, there are details of the detector setup used in experiment that are unknown. The two components which have the largest potential for affecting the overall performance of the detector are the crystal dimensions and moderator details. It was shown that detection

efficiency increased strongly with crystal volume, which allowed for simulated efficiencies comparable to measured ones. The details of the moderators used have potential for greatly affecting detector performance. This is confirmed by the significant spike in the response curves at low energies and the ability of the moderator to shift the energy of impinging neutrons.

A.   FUTURE RESEARCH

This model of the candidate crystal set and detection system using MCNP is the first computational approach at NPS in this research effort and will hopefully serve as a base model on which future efforts can build. A goal for future modeling of these crystals should be a full simulation of the scintillation process, from the emission of fast neutrons at the source to the collection and detection of photons at the PMT. This will include a reliable photon creation in MCNP, which requires a linearity curve that relates energy deposition to number of optical photons created. This linearity curve can be obtained experimentally with the crystals at NPS.

This research effort might also benefit from computational study apart from MCNP. MCNP simulation of optical emission of scintillators does not account for the LET dependence of the neutron-induced recoil nuclei or the difference in electron LET as the electrons slow down [17]. An investigation of other methods or codes to simulate the delayed response of the scintillator crystals would supplement the MCNP model.

THIS PAGE INTENTIONALLY LEFT BLANK

LIST OF REFERENCES

[1]   G. W. Bush, Office of the White House. (Sept. 17, 2002). *National Security Strategy of the United States of America.* [Online]. Available: http://georgewbush-whitehouse.archives.gov/nsc/nss/2002/nss5.html

[2]   B. W. Bennett and R. A. Love, "Initiatives and challenges in consequence management after a WMD attack." USAF Counter Proliferation Center, Aug. 2004. http://www.au.af.mil/au/awc/awcgate/cpc-pubs/love.pdf. Accessed April 2, 2015.

[3]   Department of Defense. *Defense Threat Reduction Agency & USSTRATCOM Center for Combating WMD.* Last modified March 3, 2014. Available: http://www.dtra.mil. Accessed April 2, 2015.

[4]   V. D. Ryzhikov *et al.,* "The use of fast and thermal neutron detectors based on oxide scintillators in inspection systems for prevention of illegal transportation of radioactive substances," *IEEE Transactions on Nuclear Science*, vol. 57, no. 5, pp. 1–5, Oct. 2010.

[5]   V. D. Ryzhikov *et al.,* "New neutron detectors based on inorganic scintillators using inelastic scattering," in *IEEE Nuclear Science Symp.*, Orlando, FL, 2009, pp. 1978–1982.

[6]   A. V. Bushuev, *Experimental Reactor* Physics, MIFE (Moscow Institute of Physics and Engineering), Moscow, 2008, p. 280.

[7]   X-5 Monte Carlo Team, *MCNP- A General Monte Carlo N-Particle Transport Code, Version 5. Vol II: User's Guide*. April 24, 2003. Revised 2/1/2008.

[8]   D. Reilly, N. Ensslin, and H. Smith, Jr., *Passive Nondestructive Assay of Nuclear Materials* (PANDA). Office of Nuclear Regulatory Research. March 1991.

[9]   J. B. Birks, *The Theory and Practice of Scintillation Counting*. New York: Pergamon Press, 1964, pp. 15–38, 68–76.

[10]   G. Knoll, *Radiation Detection and Measurement,* 3rd ed. Hoboken, NJ: John Wiley & Sons, 2000. pp. 30–57,113–117, 231–247, 505–553.

[11]   K. Krane, *Introductory Nuclear Physics.* Hoboken, NJ: John Wiley & Sons, 1988, pp. 444–476.

[12]   H.-C. Schults-Coulon, "Scintillation detectors: particle detection via luminescence." Kirchhoff Institute of Physics. Available: http://www.kip.uni-heidelberg.de/~coulon/Lectures/Detectors/Free_PDFs/Lecture4.pdf Accessed 5 April 2015.

[13]   J. M. Hammersley and D. C. Handscomb, *Monte Carlo Methods*. 1st ed. Boundary
        Row, London: Chapman & Hall. 1964, pp.1–55.

[14]   M. H. Kalos and P. A. Whitlock, *Monte Carlo Methods, Vol I: Basics*. New York:
        John Wiley & Sons, Inc. 1986, pp. 1–71.

[15]   V. D. Ryzhikov *et al.,* "High efficiency method of fast neutron detection by oxide
        scintillators for detection systems of fissionable radioactive
        substances," *Advancements in Nuclear Instrumentation Measurement Methods
        and their Applications (ANIMMA), 2011 2nd International Conference on* , vol.,
        no., pp.1,7, 6–9 June 2011

[16]   P. R. Rusiecki, "Characterization of heavy oxide inorganic scintillator crystals for
        direct detection of fast neutrons based on inelastic scattering." NPS. March, 2015.
        pp. 1–30.

[17]   Z. R. Harvey, "Neutron flux and energy characterization of plutonium-berylium
        isotopic neutron source by Monte Carlo simulation with verification by neutron
        activation analysis" (2010). UNLV Theses/Dissertations/Professional
        Papers/capstones. Paper 900.

[18]   T. Goorley. Private communication. September 2014.

INITIAL DISTRIBUTION LIST

1. Defense Technical Information Center
    Ft. Belvoir, Virginia

2. Dudley Knox Library
    Naval Postgraduate School
    Monterey, California